TKK Dissertations 96
Espoo 2007

ELECTROMAGNETIC FIELDS IN NANOSCALE STRUCTURES: EFFECTS OF POLARIZATION AND SPATIAL COHERENCE

Doctoral Dissertation

Jari Lindberg

Helsinki University of Technology
Department of Engineering Physics and Mathematics
Optics and Molecular Materials

TKK Dissertations 96
Espoo 2007

ELECTROMAGNETIC FIELDS IN NANOSCALE STRUCTURES: EFFECTS OF POLARIZATION AND SPATIAL COHERENCE

Doctoral Dissertation

Jari Lindberg

Dissertation for the degree of Doctor of Science in Technology to be presented with due permission of the Department of Engineering Physics and Mathematics for public examination and debate in Large Seminar Hall of Micronova at Helsinki University of Technology (Espoo, Finland) on the 9th of November, 2007, at 12 noon.

Helsinki University of Technology
Department of Engineering Physics and Mathematics
Optics and Molecular Materials

Teknillinen korkeakoulu
Teknillisen fysiikan ja matematiikan osasto
Optiikka ja molekyylimateriaalit

Distribution:
Helsinki University of Technology
Department of Engineering Physics and Mathematics
Optics and Molecular Materials
P.O. Box 3500
FI - 02015 TKK
FINLAND
URL: http://omm.tkk.fi/
Tel. +358-9-451 3153
Fax +358-9-451 3155
E-mail: jari.lindberg@tkk.fi

ISBN 978-951-22-9026-0
ISBN 978-951-22-9027-7 (PDF)
ISSN 1795-2239
ISSN 1795-4584 (PDF)
URL: http://lib.tkk.fi/Diss/2007/isbn9789512290277/

TKK-DISS-2367

Multiprint Oy
Espoo 2007

ABSTRACT OF DOCTORAL DISSERTATION	HELSINKI UNIVERSITY OF TECHNOLOGY P.O. BOX 1000, FI-02015 TKK http://www.tkk.fi
Author	
Name of the dissertation	
Manuscript submitted	Manuscript revised
Date of the defence	
Monograph	Article dissertation (summary + original articles)
Department Laboratory Field of research Opponent(s) Supervisor Instructor	
Abstract	
Keywords	
ISBN (printed)	ISSN (printed)
ISBN (pdf)	ISSN (pdf)
Language	Number of pages
Publisher	
Print distribution	
The dissertation can be read at http://lib.tkk.fi/Diss/	

VÄITÖSKIRJAN TIIVISTELMÄ	TEKNILLINEN KORKEAKOULU PL 1000, 02015 TKK http://www.tkk.fi
Tekijä	
Väitöskirjan nimi	
Käsikirjoituksen päivämäärä	Korjatun käsikirjoituksen päivämäärä
Väitöstilaisuuden ajankohta	
Monografia	Yhdistelmäväitöskirja (yhteenveto + erillisartikkelit)
Osasto Laboratorio Tutkimusala Vastaväittäjä(t) Työn valvoja Työn ohjaaja	
Tiivistelmä	
Asiasanat	
ISBN (painettu)	ISSN (painettu)
ISBN (pdf)	ISSN (pdf)
Kieli	Sivumäärä
Julkaisija	
Painetun väitöskirjan jakelu	
Luettavissa verkossa osoitteessa http://lib.tkk.fi/Diss/	

Preface

The research summarized in this work has been carried out at the Optics and Molecular Materials Laboratory of Helsinki University of Technology in the Department of Engineering Physics and Mathematics.

I am indebted to my supervisor Prof. Matti Kaivola for his guidance and support during the course of this work. I wish to thank my instructors Docent Tero Setälä and Prof. Ari T. Friberg for teaching me a lot of scientific practise and, in particular, for providing valuable insights into optical coherence theory.

I wish to express my gratitude to the Finnish Cultural Foundation, the Jenny and Antti Wihuri foundation, and the Academy of Finland for funding my doctoral studies. The Center of Scientific Computing (CSC) is also thanked for providing the computer resources.

Espoo, May 2007

Jari Lindberg

List of Publications

This thesis is a review of the author's work on near-field optics and electromagnetic coherence theory. It consists of an overview and the following selection of the author's publications in these fields:

I. J. Lindberg, T. Setälä, M. Kaivola, and A. T. Friberg, "Degree of polarization in light transmission through a near-field probe", J. Opt. A: Pure Appl. Opt. **6**, S59–S63 (2004).

II. J. Lindberg, K. Lindfors, T. Setälä, M. Kaivola, A. T. Friberg, "Spectral analysis of resonant transmission of light through a single sub-wavelength slit", Opt. Express **12**, 623–632 (2004).

III. T. Setälä, J. Lindberg, K. Blomstedt, J. Tervo, and A. T. Friberg, "Coherent-mode representation of a statistically homogeneous and isotropic electromagnetic field in spherical volume", Phys. Rev. E **71**, 036618 (2005).

IV. J. Lindberg, T. Setälä, M. Kaivola, and A. T. Friberg, "Spatial coherence effects in light scattering from metallic nanocylinders", J. Opt. Soc. Am. A **23**, 1349–1358 (2006).

V. J. Lindberg, K. Lindfors, T. Setälä, and M. Kaivola, "Dipole-dipole interaction between molecules mediated by a chain of silver nanoparticles", J. Opt. Soc. Am. A **24**, 3427–3431 (2007).

Throughout the overview, these papers will be referred to by Roman numerals.

Author's Contribution

The research presented in this dissertation is the result of work on near-field optics and electromagnetic coherence theory carried out during the years 2003–2007 in the Optics and Molecular Materials Laboratory of Helsinki University of Technology, in collaboration with the Optics Group at the Royal Institute of Technology in Stockholm.

The author has had a major role in all aspects of the research work. He has performed all the calculations and numerical implementations reported in Papers I, II, IV, and V, and has strongly contributed to the analytical and numerical calculations of Paper III. The author has played a central role in the interpretation of the results of Papers I-V. He has written the first manuscripts of Papers I, II, IV, and V, and actively participated in writing Paper III.

Other publications by the author or to which the author has contributed:

- M. Hautakorpi, J. Lindberg, T. Setälä, and M. Kaivola, "Rotational frequency shifts in partially coherent optical fields", J. Opt. Soc. Am. A **23**, 1159–1163 (2006).

Contents

Preface **vii**

List of Publications **viii**

Author's Contribution **ix**

1 Introduction **1**

2 Theoretical methods in electromagnetic theory **4**
2.1 Maxwell's equations 4
2.2 Dyadic Green's function 7
2.3 Coupled-dipole method 8
2.4 Boundary-integral method 9
2.5 Angular spectrum representation 15

3 Electromagnetic theory of optical coherence **17**
3.1 Cross-spectral density tensors 17
3.2 Degree of polarization 19
3.3 Electromagnetic degree of coherence 22
3.4 Coherent-mode representation 23

4 Electromagnetic fields in nanostructures **27**
4.1 Scanning near-field optical microscopy 27
4.2 Enhanced optical transmission 29
4.3 Plasmon resonances in metal nanoparticles 32
4.4 Molecules in nanostructures 34

5 Coherence properties of optical near fields **37**

6 Summary and conclusions **41**

References **43**

Abstracts of Publications I-V **57**

1 Introduction

Nanophotonics studies light-matter interactions in nanometer-scale structures below the diffraction limit of light [1–3]. The basic concept of nanophotonics is the optical near field which is characterized by the strong presence of evanescent (non-radiative) waves. These waves are significant only within the distance of the wavelength of light from the surface of a light emitting or scattering object. The evanescent waves play an essential role in the design and characterization of components for nanotechnology. In particular, breaking the diffraction limit of light requires the detection of evanescent waves. This is the basic principle in scanning near-field optical microscopy (SNOM) [4–8] which is an important tool in investigations of optical near fields and nanoscale structures.

Evanescent waves play an essential role also in studies of surface plasmon polaritons [9–13] which are coupled oscillations of electromagnetic field and surface charges at metal-dielectric interface. These waves decay exponentially away from the interface and hence are highly localized on the surface. The localization and other properties of surface plasmon polaritons make them attractive for nano-optical applications. Indeed, surface plasmon-based photonics, i.e., plasmonics, has currently become an extremely active area of research. In addition to surface plasmon polaritons on planar surfaces, there exist also localized surface plasmons on metallic nanoparticles and nanowires. Surface plasmons can produce highly localized and strong electromagnetic fields. They can be utilized in guiding electromagnetic energy at sub-wavelength scale. This can be achieved along metallic nanowires where light can be transported over distances of a few micrometers [13]. The high ohmic losses in these structures limit the maximum propagation length. The losses can be smaller in an array consisting of metallic nanoparticles due to the reduced metallic volume [13]. Metal nanoparticles exhibit (localized) plasmon resonances at certain wavelengths, and in a chain of such particles the excitation can couple from one particle to another leading to energy transfer at sub-wavelength scale.

In addition to plasmon waveguides there exists considerable interest in other components for controlling surface plasmons – mirrors, switches, modulators, couplers, and resonators. The properties of surface plasmons can be modified by nanostructuring the metal surface. On a periodically structured metal film surface it is possible even to have a full photonic band gap for surface plasmon modes thus preventing them from travelling in any in-plane direction [11]. Furthermore, surface plasmons account for the enhanced optical transmission observed in nanohole arrays on metal films. The transmission properties can also be influenced by corrugating the metal film, and it is possible to have a fairly collimated beam of light emerging from a sub-wavelength aperture.

Integrating plasmonic components on a single substrate would create an all-plasmonic chip that in the future could allow merging optics and electronics at

nanoscale. Light would first be coupled into surface plasmons, which propagate through the plasmonic chip, and are then converted back to light again [11]. Strong local field enhancement associated with the plasmon resonance and the sensitivity of the resonance to the surrounding environment has been utilized in sensor applications, such as in detecting biomolecules, and in surface-enhanced Raman spectroscopy (SERS) where single molecule detection has been achieved [14, 15].

The existence of surface plasmon modes on planar metallic surfaces has also important implications for the radiative properties of molecules near metal surfaces [16–18]. The spontaneous emission rate of a molecule is modified near a planar interface due to the interaction of the emitter with the field which is reflected back from the interface. The emission from the molecule can either be enhanced or inhibited depending on whether the reflected field is in phase or out of phase at the emitter site. Surface plasmons have been utilized to improve light-emission efficiencies of semiconductor-based light emitting diodes by coating the semiconductor structures with a thin metal film [13]. Furthermore, not only the radiative decay rate but also the interaction of molecules with each other is strongly affected in the presence of metal films. It has been demonstrated that in fluorescence resonance energy transfer (FRET), where the excitation of one molecule is transferred to another molecule non-radiatively, can be mediated by surface plasmons through metal films. Emission from molecules and their mutual interactions can thus be affected by tailoring the nanostructures in which the molecules are embedded.

The results mentioned above have mainly been found for optical near fields which are fully polarized and spatially fully coherent. From the practical point of view it is, of course, often appropriate to ignore the possibility of partial polarization and partial coherence, and to consider the near field as a monochromatic, fully deterministic field. However, the inclusion of partial polarization and partial coherence in the analysis of optical near fields may lead to appearance of new fundamental physical phenomena as reported in recent papers [19–22]. Firstly, in contrast to the conventional half-wavelength lower limit of the spatial coherence length, the coherence length in the near field of a thermal source may be a fraction of light's wavelength or it may extend over several tens of wavelengths when surface plasmon or phonon polaritons are excited [19, 20]. Secondly, the plasmon excitations may lead to a quasi-monochromatic spectrum for the near field although the source and far field have wide-band spectra [21]. Thirdly, even if the source is highly unpolarized, the near field can be highly polarized in the presence of surface plasmons [22]. A key issue that so far has hindered the analysis of fluctuating near fields is the lack of suitable theoretical methods which would hold for general, three-dimensional electromagnetic fields such as optical near fields. Indeed, the traditional concepts of optical coherence theory are, as a rule, valid only for scalar fields or planar, two-dimensional electromagnetic fields [23–27], e.g., optical beams or far fields where the evanescent waves play no role. The situation has, however, started to change

very recently and some basic concepts such as the degree of polarization, electromagnetic degree of coherence and electromagnetic theory of coherent modes have been extended to full 3D vectorial fields.

In this Thesis, the (partial) polarization and spatial coherence properties of optical near fields are studied. The transmission of partially polarized light through a near-field probe is analyzed in terms of the 3D degree of polarization. The enhanced transmission of light through a single sub-wavelength slit is also investigated. The electromagnetic coherence theory is applied to study plasmon resonances in metallic nanocylinders, and their effect on the degree of polarization and the degree of coherence, as well as on the electromagnetic energy transfer in the optical near field is assessed. The fluorescence resonance energy transfer mediated by plasmon resonant metallic nanoparticles is also addressed.

This compendium to the thesis is organized as follows: In Sec. 2 some basic theoretical methods for analyzing electromagnetic fields are presented. These methods apply to deterministic fields such as those studied in Papers II and V, but they can also be utilized in connection with random electromagnetic fields as is done in Papers I and IV. Section 3 introduces the essential basic concepts of optical coherence theory pertaining to scalar and planar, two-dimensional electromagnetic fields. In particular, the extension of these topics to full 3D electromagnetic fields are presented and their physical interpretation is discussed. These concepts are used to characterize partially polarized and partially coherent electromagnetic near fields in Papers I and IV. Also, the representation of a partially coherent field as a superposition of mutually uncorrelated coherent modes, i.e. the coherent-mode representation, for both scalar and electromagnetic fields is presented. In Paper III, for the first time, a fully 3D coherent-mode representation is derived for a certain class of random electromagnetic fields. The coherent-mode representation is also utilized in the calculations of scattering of a partially polarized, partially coherent field from metallic nanocylinders in Paper IV. Section 4 discusses the physical properties of nano-optical systems which are the subjects of Papers I, II, IV, and V. The spatial coherence properties of optical near fields, which so far have received relatively little attention, are discussed in Sec. 5. The essential role of evanescent waves and surface plasmons in the coherence phenomena of optical near fields is depicted.

2 Theoretical methods in electromagnetic theory

In this section, a brief overview of the basic concepts of the theoretical methods in electromagnetic theory is given. The emphasis is on the space-frequency domain methods, and in particular on the techniques that are employed in Papers I-V.

2.1 Maxwell's equations

The microscopic Maxwell's equations determine the electric and magnetic fields which are generated by a distribution of discrete charges and currents in vacuum. Macroscopic electrodynamics deals with fields in matter in terms of local spatial averages of these microscopic fields [28]. In the macroscopic Maxwell's equations the charge and current densities are considered as continuous functions and the equations are written in SI units as [1]

$$\nabla \cdot \mathbf{D}(\mathbf{r},t) = \rho(\mathbf{r},t), \tag{1}$$
$$\nabla \cdot \mathbf{B}(\mathbf{r},t) = 0, \tag{2}$$
$$\nabla \times \mathbf{E}(\mathbf{r},t) = -\frac{\partial \mathbf{B}(\mathbf{r},t)}{\partial t}, \tag{3}$$
$$\nabla \times \mathbf{H}(\mathbf{r},t) = \mathbf{J}(\mathbf{r},t) + \frac{\partial \mathbf{D}(\mathbf{r},t)}{\partial t}. \tag{4}$$

Here $\mathbf{E}$ and $\mathbf{H}$ are the electric and magnetic fields, respectively, and $\mathbf{D}$ is the electric displacement and $\mathbf{B}$ the magnetic induction. The quantities ρ and $\mathbf{J}$ represent the density of charges and currents that are present in the medium. The vectors $\mathbf{D}$ and $\mathbf{B}$ take into account the response of the medium to the electromagnetic field. They are connected to the polarization, $\mathbf{P}$, and magnetization, $\mathbf{M}$, induced in the medium by an electromagnetic field through the relations,

$$\mathbf{D}(\mathbf{r},t) = \epsilon_0 \mathbf{E}(\mathbf{r},t) + \mathbf{P}(\mathbf{r},t), \tag{5}$$
$$\mathbf{B}(\mathbf{r},t) = \mu_0 \left[\mathbf{H}(\mathbf{r},t) + \mathbf{M}(\mathbf{r},t)\right], \tag{6}$$

where the quantities ϵ_0 and μ_0 are the vacuum permittivity and permeability, respectively.

Constitutive relations

The relation between $\mathbf{E}$ and $\mathbf{D}$ ($\mathbf{B}$ and $\mathbf{H}$) can, in general, be rather complicated. In a linear and isotropic medium the electric displacement $\mathbf{D}$ can be written as [1, 28]

$$\mathbf{D}(\mathbf{r},t) = \int_{-\infty}^{t}\int_{-\infty}^{\infty} \epsilon(\mathbf{r}-\mathbf{r}', t-t')\mathbf{E}(\mathbf{r}',t)\mathrm{d}\mathbf{r}'\mathrm{d}t', \tag{7}$$

where $\epsilon(\mathbf{r}-\mathbf{r}', t-t')$ is a response function which vanishes for $t' > t$ due to causality. The electric displacement $\mathbf{D}(\mathbf{r}, t)$ at point $\mathbf{r}$ and time t depends on the electric field at $\mathbf{r}$ but also on the field values at neighboring points $\mathbf{r}'$ at previous instants of time t'. The relation of $\mathbf{D}$ and $\mathbf{E}$ is thus non-local and the medium is said to be spatially dispersive.

By applying Fourier transform to Eq. (7) with respect to $\mathbf{r}$ and t, one obtains

$$\tilde{\mathbf{D}}(\mathbf{k}, \omega) = \epsilon(\mathbf{k}, \omega)\tilde{\mathbf{E}}(\mathbf{k}, \omega), \tag{8}$$

where $\epsilon(\mathbf{k}, \omega)$ is the dielectric function of the medium at angular frequency ω, and tilde denotes the Fourier transformed field variables. The effects of spatial dispersion, i.e., the dependence of the dielectric function on the wavevector $\mathbf{k}$, can be seen, for example, at interfaces between different media or in metallic objects with dimensions comparable to the mean-free path of electrons [1, 29]. However, in many cases of interest in nano-optics the non-local effects are weak and can be ignored [1]. For local (spatially non-dispersive), homogeneous, isotropic, and linear media, which may be temporally dispersive, i.e., having material parameters that depend on ω, the constitutive relations assume the form [1]

$$\begin{aligned} \tilde{\mathbf{D}}(\mathbf{r}, \omega) &= \epsilon(\omega)\tilde{\mathbf{E}}(\mathbf{r}, \omega) && (9) \\ \tilde{\mathbf{B}}(\mathbf{r}, \omega) &= \mu(\omega)\tilde{\mathbf{H}}(\mathbf{r}, \omega), && (10) \end{aligned}$$

with $\epsilon(\omega) = \epsilon_0\epsilon_r(\omega)$ and $\mu(\omega) = \mu_0\mu_r(\omega)$ denoting the permittivity and permeability respectively. Here $\epsilon_r(\omega)$ and $\mu_r(\omega)$ are the relative permittivity and permeability of the medium, respectively. The relative permeability for all media is practically equal to one at optical frequencies [1].

The total current density $\mathbf{J}$ in Eq. (4) can be split into a source current density $\mathbf{J}_s$ and an induced conduction current density $\mathbf{J}_c$. The conduction current density is related to the electric field via conductivity $\sigma(\omega)$ of the medium as [1]

$$\tilde{\mathbf{J}}_c(\mathbf{r}, \omega) = \sigma(\omega)\tilde{\mathbf{E}}(\mathbf{r}, \omega). \tag{11}$$

Boundary conditions

On the interface of two media, Maxwell's equations satisfy the following boundary conditions [31]

$$\begin{aligned} \mathbf{n} \times (\mathbf{E}_2 - \mathbf{E}_1) &= \mathbf{0}, && (12) \\ \mathbf{n} \times (\mathbf{H}_2 - \mathbf{H}_1) &= \mathbf{K}, && (13) \\ \mathbf{n} \cdot (\mathbf{D}_2 - \mathbf{D}_1) &= \rho_s, && (14) \\ \mathbf{n} \cdot (\mathbf{B}_2 - \mathbf{B}_1) &= 0, && (15) \end{aligned}$$

which are usually deduced from the integral form of Maxwell's equations. The subscripts refer to medium 1 and medium 2, and $\mathbf{n}$ denotes the normal vector pointing from medium 1 into medium 2. Furthermore, $\mathbf{K}$ is the surface current density and ρ_s denotes the surface charge density. The four boundary conditions are not independent, since they are connected via Maxwell's equations. The boundary conditions for the normal components are automatically satisfied if the boundary conditions for the tangential components hold everywhere on the boundary and Maxwell's equations are fulfilled in both domains [1]. The surface current $\mathbf{K}$ is zero in the case of any real material, i.e. for materials that are not perfectly conducting, implying that the tangential component of the magnetic field is continuous across the interface [30]. It is often a useful idealization to treat the material as being perfectly conducting as this can significantly simplify the calculations.

Time-harmonic fields

A time-harmonic field oscillates at a single constant frequency and is hence called also monochromatic field. In reality, no wave is strictly monochromatic since real waves always comprise a band of frequencies. However, time-harmonic fields have a special significance since a field with an arbitrary time-dependence can be synthesized as a superposition of time-harmonic fields. Furthermore, the temporal dispersion in a system can be taken into account by considering the wave propagation for time-harmonic fields at different frequencies separately. A monochromatic electric field can be written as

$$\mathbf{E}(\mathbf{r},t) = \mathrm{Re}\left\{\mathbf{E}(\mathbf{r})\exp(-\mathrm{i}\omega t)\right\}. \tag{16}$$

By assuming the harmonic time dependence for all the fields in Maxwell's equations, one finds that the spatial parts of the fields satisfy

$$\begin{aligned}
\nabla\cdot\mathbf{D}(\mathbf{r}) &= \rho(\mathbf{r}), &(17)\\
\nabla\cdot\mathbf{B}(\mathbf{r}) &= 0, &(18)\\
\nabla\times\mathbf{E}(\mathbf{r}) &= \mathrm{i}\omega\mathbf{B}(\mathbf{r}), &(19)\\
\nabla\times\mathbf{H}(\mathbf{r}) &= \mathbf{J}(\mathbf{r}) - \mathrm{i}\omega\mathbf{D}(\mathbf{r}), &(20)
\end{aligned}$$

where the complex field amplitudes and the material parameters depend on the angular frequency ω although this dependence is often not explicitly depicted [1]. These equations for the spatial parts of the time-harmonic field, e.g. for $\mathbf{E}(\mathbf{r})$, are similar in form to the equations of the spectral components of arbitrary time-dependent fields $\tilde{\mathbf{E}}(\mathbf{r},\omega)$ and they are in fact identical under formal time-independent operations, although these fields have different units and differ also in their interpretation [30].

From Maxwell's curl equations (3) and (4), one can derive the wave equations for the electric and magnetic field. With the help of the constitutive relations, and by introducing the complex dielectric constant with the substitution [1]

$$[\epsilon_r + \mathrm{i}\sigma/(\omega\epsilon_0)] \rightarrow \epsilon_r, \tag{21}$$

one obtains the wave equation in a linear, homogeneous, and isotropic medium for the spatial part of the electric and magnetic fields as

$$\nabla \times \nabla \times \mathbf{E}(\mathbf{r}) - k^2\mathbf{E}(\mathbf{r}) = \mathrm{i}\omega\mu_0\mu_r\mathbf{J}_s(\mathbf{r}), \tag{22}$$

$$\nabla \times \nabla \times \mathbf{H}(\mathbf{r}) - k^2\mathbf{H}(\mathbf{r}) = \nabla \times \mathbf{J}_s(\mathbf{r}), \tag{23}$$

where $k = k_0 n$ is the wavenumber. Here $k_0 = \omega/c$ is the vacuum wavenumber with c being the speed of light in vacuum, and $n = \sqrt{\epsilon_r\mu_r}$ is the refractive index of the medium.

2.2 Dyadic Green's function

To obtain a solution to the wave equation, it is often useful to work with the dyadic Green's function or the field propagator $\overleftrightarrow{G}(\mathbf{r}, \mathbf{r}')$ [31]. As it will be shown, the dyadic Green's tensor gives at position $\mathbf{r}$ the electric field $\mathbf{E}$ which is generated by a point dipole at $\mathbf{r}'$.

The propagator $\overleftrightarrow{G}(\mathbf{r}, \mathbf{r}')$ satisfies the wave equation with a delta function as source term [31]

$$\nabla \times \nabla \times \overleftrightarrow{G}(\mathbf{r}, \mathbf{r}') - k^2\,\overleftrightarrow{G}(\mathbf{r}, \mathbf{r}') = \delta(\mathbf{r} - \mathbf{r}'). \tag{24}$$

The solution to the wave equation of Eq. (22), when a source distribution $\mathbf{J}(\mathbf{r})$ is located in volume V, can be expressed as

$$\mathbf{E}(\mathbf{r}) = \mathbf{E}_0(\mathbf{r}) + \mathrm{i}\omega\mu \int_V \overleftrightarrow{G}(\mathbf{r}, \mathbf{r}') \cdot \mathbf{J}(\mathbf{r}')\mathrm{d}^3r', \tag{25}$$

where $\mathbf{E}_0(\mathbf{r})$ is the solution of the homogeneous wave equation and $\mathbf{r}$ is a point located outside V. In a typical scattering problem $\mathbf{E}_0(\mathbf{r})$ is the incident field which excites polarization currents in the scatterer bounded by volume V.

The free-space propagator can be expressed as [31]

$$\overleftrightarrow{G}(\mathbf{r}, \mathbf{r}') = \left(\overleftrightarrow{U} + \frac{1}{k^2}\nabla\nabla\right) G(\mathbf{r}, \mathbf{r}'), \tag{26}$$

with $\overleftrightarrow{U}$ denoting the unit tensor and $G(\mathbf{r}, \mathbf{r}')$ being the scalar Green's function

$$G(\mathbf{r}, \mathbf{r}') = \frac{\exp(\mathrm{i}k|\mathbf{r} - \mathbf{r}'|)}{4\pi|\mathbf{r} - \mathbf{r}'|}, \tag{27}$$

which satisfies

$$(\nabla^2 + k^2)G(\mathbf{r}, \mathbf{r}') = -\delta(\mathbf{r} - \mathbf{r}'). \tag{28}$$

Sometimes one is interested in the field *inside* a source region. This requires the use of principal volume to exclude the singularity of $G(\mathbf{r}, \mathbf{r}')$ at $\mathbf{r} = \mathbf{r}'$ [32,33]. The depolarization of the principal volume results in an additional term in the volume integral equation which depends on the geometrical shape of the volume. Furthermore, a second correction term arises in numerical schemes due to the finite size of the principal volume [34].

In nano-optics one is often interested in the electric field which is generated by an electric point dipole of dipole moment $\mathbf{p}$ located at $\mathbf{r}'$ in vacuum, for which the current density has the form $\mathbf{J}(\mathbf{r}) = -\mathrm{i}\omega\mathbf{p}\delta(\mathbf{r} - \mathbf{r}')$. The field is given in terms of the dyadic Green's function as [1]

$$\mathbf{E}(\mathbf{r}) = \omega^2\mu_0 \overleftrightarrow{G}(\mathbf{r}, \mathbf{r}') \cdot \mathbf{p}. \tag{29}$$

Sometimes the factor $\omega^2\mu_0$ is included in the definition of the Green's tensor [35]. As the dyadic Green's tensor characterizes the electromagnetic response of the system, several important quantities such as the local density of states of the electromagnetic field, and the environment-induced changes in the radiative properties of molecules can be directly obtained once the dyadic Green's function of the system is known.

2.3 Coupled-dipole method

Equation (25) gives the electric field outside a source distribution. In practice, the volume integral can be approximated as a sum over finite volume elements ΔV. In the coupled-dipole method one considers the field that excites a given volume element ΔV [1]. In particular, for a system which consists of N small individual scatterers, e.g. of small metal particles as in Paper V, each of these is considered as a point dipole. Larger particles can be handled by dividing them into smaller dipolar subvolumes.

Treating each of the N coupled volume elements as a point dipole yields for the electric field outside the particles [1]

$$\mathbf{E}(\mathbf{r}, \omega) = \mathbf{E}_0(\mathbf{r}, \omega) + \omega^2\mu \sum_{n=1}^{N} \overleftrightarrow{G}(\mathbf{r}, \mathbf{r}_n, \omega) \cdot \mathbf{p}_n. \tag{30}$$

The dipole moment $\mathbf{p}_n$ is proportional to the exciting field $\mathbf{E}_{\mathrm{exc}}(\mathbf{r}_n, \omega)$ which consists of $\mathbf{E}_0(\mathbf{r}_n, \omega)$ and the fields scattered by the other particles

$$\mathbf{p}_n = \overleftrightarrow{\alpha}_n(\omega) \cdot \mathbf{E}_{\mathrm{exc}}(\mathbf{r}_n, \omega). \tag{31}$$

Here $\overleftrightarrow{\alpha}_n(\omega)$ is the polarizability tensor of particle n. The exciting field $\mathbf{E}_{\mathrm{exc}}(\mathbf{r}_n, \omega)$ is not in general equal to the field that is actually present at the location of the particle as it neglects the contribution due to self-interaction [34]. However, the influence of the particle to the field at its center can be included in the polarizability tensor. Combining Eqs. (30) and (31) one finds that the unknown dipole moments are determined by the following system of coupled equations [34]

$$\mathbf{p}_k = \overleftrightarrow{\alpha}_k\,(\omega) \cdot \mathbf{E}_0(\mathbf{r}_k, \omega) + \sum_{\substack{n=1 \\ n \neq k}}^{N} \overleftrightarrow{\alpha}_k\,(\omega) \cdot \overleftrightarrow{G}_0\,(\mathbf{r}_k, \mathbf{r}_n, \omega) \cdot \mathbf{p}_n, \tag{32}$$

where $k = 1, \ldots, N$. In practice, this equation is solved numerically, and once the dipole moments are known, the electric field outside the particles can be calculated from Eq. (30).

2.4 Boundary-integral method

In the case of scattering problems in systems that are invariant in one direction, say z, Maxwell's equations reduce to two independent sets of equations [23, 30]. These sets describe a transverse electric (TE) field, having components (E_z, H_x, H_y), and a transverse magnetic (TM) field with components (H_z, E_x, E_y). An electromagnetic field can be decomposed into TE- and TM-components, which can be analyzed separately since they are not coupled. The TE and TM polarizations can both be described in terms of a single scalar variable ψ, which represents the z-component of the electric field in the case of TE-polarization and the z-component of the magnetic field in the case of TM-polarization. The decomposition of the field into its TM and TE components allows the solution to a scattering problem be expressed as an integral equation for the scalar field ψ, which is utilized in Papers I, II, and IV. From the vector wave equations in the absence of the source terms, Eqs. (22) and (23), we obtain the scalar Helmholtz equation for ψ as

$$(\nabla^2 + k^2)\psi(\mathbf{r}) = 0. \tag{33}$$

The Green's function for the two-dimensional (2D) scalar Helmholtz equation is given by [31]

$$G(\mathbf{r}, \mathbf{r}') = \frac{\mathrm{i}}{4} H_0^{(1)}(k|\mathbf{r} - \mathbf{r}'|), \tag{34}$$

where $H_0^{(1)}$ is the zeroth order Hankel function of the first kind, and $\mathbf{r}$ and $\mathbf{r}'$ are referred to as the field and the source point, respectively. The 2D Green's function satisfies the inhomogeneous Helmholtz equation with a δ-function source term in Eq. (28), where in the 2D case the operator is $\nabla^2 = \partial^2/(\partial x^2) + \partial^2/(\partial y^2)$.

The solution to the Helmholtz equation in a (closed) region can be obtained in terms of an integral over the boundaries of the region. The integral equation is derived by applying the Green's theorem [30]

$$\int_A \left(G\nabla^2\psi - \psi\nabla^2 G\right) \mathrm{d}a = \oint_s \left[G\frac{\partial}{\partial n}\psi - \psi\frac{\partial}{\partial n}G\right] \mathrm{d}s, \tag{35}$$

where $\partial/\partial n$ denotes the derivative in the direction of the outward normal vector to the curve s bounding the closed region A. By excluding the singular point $\mathbf{r} = \mathbf{r}'$ from A with a circle of infinitesimal radius, one obtains the boundary-integral equation for the scalar field $\psi(\mathbf{r})$ inside the region A as [36]

$$\psi(\mathbf{r}) = \oint_s \left[G(\mathbf{r},\mathbf{r}')\frac{\partial}{\partial n'}\psi(\mathbf{r}') - \psi(\mathbf{r}')\frac{\partial}{\partial n'}G(\mathbf{r},\mathbf{r}')\right] \mathrm{d}s'. \tag{36}$$

The normal derivative of the Green's function in this equation is explicitly written as

$$\frac{\partial}{\partial n'}G(\mathbf{r},\mathbf{r}') = \frac{\mathrm{i}k}{4}H_1^{(1)}(k|\mathbf{r}-\mathbf{r}'|)\cos\alpha, \tag{37}$$

where α is the angle between the normal vector and the vector $\mathbf{r} - \mathbf{r}'$.

In a system consisting of multiple sub-domains of a homogeneous and isotropic material, the field in each sub-domain l can be calculated in terms of the corresponding boundary values according to Eq. (36) as

$$\psi_l(\mathbf{r}) = \oint_{s_l} \left[G_l(\mathbf{r},\mathbf{r}')\frac{\partial}{\partial n'}\psi_l(\mathbf{r}') - \psi_l(\mathbf{r}')\frac{\partial}{\partial n'}G_l(\mathbf{r},\mathbf{r}')\right] \mathrm{d}s'. \tag{38}$$

The boundary conditions of Eqs. (12)–(15) connect the values of ψ and its normal derivative between two adjacent regions. In the case of media that are not perfectly conducting ($\mathbf{K} = 0$) and in the absence of other than polarization induced charges ($\rho_s = 0$), it follows that a TE-polarized field ψ and its normal derivative satisfy at the boundary of media 1 and 2 the equations

$$\psi_1 = \psi_2, \tag{39}$$

$$\frac{1}{\mu_1}\frac{\partial\psi_1}{\partial n_1} = -\frac{1}{\mu_2}\frac{\partial\psi_2}{\partial n_2}. \tag{40}$$

For a TM-polarized field one has

$$\psi_1 = \psi_2, \tag{41}$$

$$\frac{1}{\epsilon_1}\frac{\partial\psi_1}{\partial n_1} = -\frac{1}{\epsilon_2}\frac{\partial\psi_2}{\partial n_2}. \tag{42}$$

Poynting vector and the optical theorem

One is often interested in the direction and magnitude of energy flow in nano-optical systems. Within this Thesis, this is of particular interest in analyzing the enhanced optical transmission through sub-wavelength apertures in metal films (see Sec. 4.2) which is the topic of Paper II. The time-averaged Poynting vector which characterizes the net power flux density is [1]

$$\langle \mathbf{S}(\mathbf{r}) \rangle = \frac{1}{2} \mathrm{Re} \left\{ \mathbf{E}(\mathbf{r}) \times \mathbf{H}^*(\mathbf{r}) \right\}, \tag{43}$$

which in terms of the scalar function ψ for a TE-polarized field can be written as

$$\langle \mathbf{S}_{\mathrm{TE}}(\mathbf{r}) \rangle = \frac{1}{2\omega} \mathrm{Re} \left\{ \frac{\mathrm{i}}{\mu^*(\mathbf{r},\omega)} \psi(\mathbf{r}) \nabla \psi^*(\mathbf{r}) \right\}, \tag{44}$$

and as

$$\langle \mathbf{S}_{\mathrm{TM}}(\mathbf{r}) \rangle = \frac{1}{2\omega} \mathrm{Re} \left\{ -\frac{\mathrm{i}}{\epsilon(\mathbf{r},\omega)} \psi^*(\mathbf{r}) \nabla \psi(\mathbf{r}) \right\}, \tag{45}$$

for a TM-polarized field.

In a typical 2D scattering problem a plane-wave is incident on a finite-sized scatterer which is embedded in a non-absorbing medium. One is often interested in the power P which is extracted from the incident wave ψ_{inc}. The total power consists of two parts: the absorbed power P_{abs} and the scattered power P_{sc}. The power P_{abs} absorbed by the scatterer is obtained by integrating the Poynting vector over the boundary s of the scatterer

$$P_{\mathrm{abs}} = -\int_s \langle \mathbf{S}(\mathbf{r}) \rangle \cdot \hat{n} \mathrm{d}s. \tag{46}$$

The scattered power P_{sc} is calculated by integrating the time-averaged Poynting vector of the scattered field $\psi_{\mathrm{sc}} = \psi - \psi_{\mathrm{inc}}$ over a cylindrical boundary s' enclosing the scatterer

$$P_{\mathrm{sc}} \;\; = \;\; \int_{s'} \langle \mathbf{S}_{\mathrm{sc}}(\mathbf{r}) \rangle \cdot \hat{n} \mathrm{d}s'. \tag{47}$$

The total extracted power normalized by the irradiance I of the incident field defines the extinction cross-section $\sigma_{\mathrm{ext}} = P/I$ which has the dimension of length [37]. The extinction cross-section is equal to the sum of the scattering and absorption cross-sections $\sigma_{\mathrm{sc}} = P_{\mathrm{sc}}/I$ and $\sigma_{\mathrm{abs}} = P_{\mathrm{abs}}/I$, respectively. The extinction cross-section can be obtained from the two-dimensional form of the optical theorem [37–39] as

follows: The total field in the far zone can be expressed in terms of the incident and scattered fields as

$$\psi(\mathbf{r}) = \psi_{\rm inc}(\mathbf{r}) + \psi_{\rm sc}(\mathbf{r}) \sim \exp(\mathrm{i}\mathbf{k}\cdot\mathbf{r}) + f(\theta,\mathbf{k})\frac{\exp(\mathrm{i}kr)}{\sqrt{r}}, \tag{48}$$

where $f(\theta,\mathbf{k})$ is the differential scattering amplitude and $r = |\mathbf{r}|$. The geometry of the scattering problem consists of a boundary at infinity and the boundary of the scatterer. The incident field satisfies the integral equation of Eq. (36) which allows the scattered field to be written as [37, 38]

$$\psi_{\rm sc}(\mathbf{r}) = \int_s \left[G(\mathbf{r},\mathbf{r}')\frac{\partial}{\partial n'}\psi_{\rm sc}(\mathbf{r}') - \psi_{\rm sc}(\mathbf{r}')\frac{\partial}{\partial n'}G(\mathbf{r},\mathbf{r}') \right] \mathrm{d}s', \tag{49}$$

where there is no contribution from the boundary at infinity since the scattered field satisfies the radiation condition [37]. By using the asymptotic form of the Hankel function [40]

$$H_0^{(1)}(z) \sim \sqrt{\frac{2}{\pi z}}\exp[\mathrm{i}(z-\pi/4)], \tag{50}$$

the scattered field in the far zone can be evaluated, and by comparison to Eq. (48) the differential scattering amplitude is seen to be [38]

$$f(\theta,\mathbf{k}) = \frac{1+\mathrm{i}}{4\sqrt{\pi k}}\int_s \exp(-\mathrm{i}r'\mathbf{k}_f\cdot\mathbf{r}') \left[\frac{\partial}{\partial n'}\psi_{\rm sc}(\mathbf{r}') + \mathrm{i}\mathbf{k}\cdot\hat{n}'\psi_{\rm sc}(\mathbf{r}') \right] \mathrm{d}s', \tag{51}$$

where $\mathbf{k}_f = (k\cos\theta, k\sin\theta)$ and θ is the detection angle. The optical theorem states that extinction (absorption and scattering) depends only on the scattering amplitude in the forward direction. By denoting $\mathbf{k}_f = \mathbf{k} = (k\cos\phi, k\sin\phi)$ the extinction cross-section can be written as [38]

$$\sigma_{\rm ext} = 2\sqrt{\frac{\pi}{k}}\mathrm{Im}\{(1-\mathrm{i})f(\theta=\phi,\mathbf{k})\}, \tag{52}$$

which for non-absorbing scatterers is equal to the scattering cross-section $\sigma_{\rm sc} = \int_0^{2\pi}|f(\theta,\mathbf{k})|^2\mathrm{d}\theta$. The scattering and absorption cross-sections are important parameters in characterizing the properties of a scatterer. For instance, in the context of this Thesis, when considering the response of metal nanocylinders to electromagnetic, these cross-sections are known to exhibit resonances for certain wavelengths when a plasmon resonance is excited (see Sec. 4.3). In particular, the wavelengths of these resonances for individual and interacting nanocylinders, a problem studied in Paper IV, are obtained by analyzing the spectral behavior of the scattering and absorption cross-sections.

Numerical implementation

The numerical solution to the boundary-integral equation can be obtained by using the boundary-element method (BEM) [41–43]. In dealing with surface-integral equations, BEM is often used synonymously with the 'method of moments' [44]. BEM has been widely employed in solving electromagnetic problems [45] including waveguide discontinuities [46], near-field microscopy [47–49], surface scattering [50], and cavity resonances [38]. Given the close analogy between the Helmholtz and Schrödinger equations [50], the surface integral formulation using BEM has also been applied to solving electronic states in semiconductor heterostructures [51, 52].

In BEM, the boundaries are discretized into finite elements. The shape of the element is determined by the node points $\mathbf{r}_i$ and the shape functions (interpolation polynomials) $N(\xi)$, e.g., for a linear element with node points at both ends of the element, we have

$$\mathbf{r}(\xi) = N_1(\xi)\mathbf{r}_1 + N_2(\xi)\mathbf{r}_2, \tag{53}$$

with $N_1(\xi) = (1-\xi)/2$, $N_2(\xi) = (1+\xi)/2$, and ξ running from -1 to $+1$. The shape functions for higher-order elements (quadratic, cubic, etc.) can be generated in a straightforward way [43]. The values of the field ψ and its normal derivative on the element are determined from the values at the nodes of the element using the interpolation functions.

In order to be able to calculate the field inside a closed region using the boundary-integral method, the field ψ and its normal derivative ψ' must be known at the boundary. To solve these two boundary unknowns, the scalar function $\psi(\mathbf{r}_i)$ is evaluated for each node $\mathbf{r}_i$ using the boundary integral of Eq. (38). The Green's function and its normal derivative have singularities at $\mathbf{r}_i = \mathbf{r}'$ which requires a special treatment. The singular point is handled by deforming the boundary around the singular point with an arc of radius ϵ and taking the limit as $\epsilon \to 0$. Using the small-argument expansions for the Hankel function and its derivative [40]

$$\lim_{z\to 0} H_0^{(1)}(z) \sim \frac{2\mathrm{i}}{\pi}\ln z, \tag{54}$$

$$\lim_{z\to 0} \frac{d}{dz}H_0^{(1)}(z) \sim \frac{2\mathrm{i}}{\pi z}, \tag{55}$$

the integral along the arc becomes [43]

$$\frac{1}{2\pi}\int \left\{-\epsilon\ln\epsilon\left[\hat{n}\cdot\nabla'\psi(\mathbf{r}')\right]|_{\mathbf{r}'=\mathbf{r}_i} + \psi_i(\mathbf{r}')|_{\mathbf{r}'=\mathbf{r}_i}\right\}\mathrm{d}\theta. \tag{56}$$

In the limit $\epsilon \to 0$, the first term vanishes and the second term gives a contribution $\Delta\theta_i/(2\pi)\psi(\mathbf{r}_i)$, where $\Delta\theta_i$ is the angle traversed around the singular point $\mathbf{r}_i$, which

for a straight segment evaluates to $\psi(\mathbf{r}_i)/2$. The boundary integral of Eq. (36) at node i can be written in a discretized form as a sum over the elements (subscript α) and element nodes (subscript j)

$$(1 - C_i)\psi_i = \sum_{\alpha} \sum_{j} \left(\mathcal{G}_{\alpha,j} \psi'_{\alpha,j} + \mathcal{H}_{\alpha,j} \psi_{\alpha,j} \right), \tag{57}$$

with $C_i = \Delta\theta_i/(2\pi)$, and $\psi_{\alpha,j}$ and $\psi'_{\alpha,j}$ denoting the field and its normal derivative at node j. The coefficients $\mathcal{G}_{\alpha,j}$ and $\mathcal{H}_{\alpha,j}$ consist of integrals involving the Green's function and its normal derivative and the interpolation functions $N_{\alpha,j}(\xi)$ over the element α.

These integrals are evaluated by using Gaussian quadratures. Integration over the element involving the singular node can be treated in a straightforward way. The singularity of the Green's function is of the logarithmic type and can be handled using a suitable quadrature [43]. The accuracy can be further improved with an appropriate coordinate transformation [53]. The integration of the term involving the normal derivative of the Green's function gives zero for a straight segment because the normal vector is perpendicular to $\mathbf{r} - \mathbf{r}'$. For a curved element, this term is also integrable as the singularity is compensated by the term

$$\cos\alpha \sim \frac{1}{2}\kappa|\mathbf{r} - \mathbf{r}'|, \tag{58}$$

where the curvature κ is finite for a smooth boundary [38].

The treatment of corner points in BEM requires some care as the normal derivatives in two elements terminating at the corner node can be different. There exist several methods for dealing with this ambiguity [43]. For example, one can pull back the nodes from the two elements so that they no longer coincide, or one can round out the corner so that the normal derivative is uniquely defined. A more sophisticated solutions involves the use of Hermite interpolation polynomials for both the field and its normal derivative instead of Lagrange interpolation. The Hermite interpolation allows imposing derivative continuity at the nodes which can also enhance the accuracy of the results [43].

Once the integrations over the elements are performed, the coefficients for each boundary node can be collected. If the number of boundary nodes is N, one has $4N$ unknowns, namely the scalar function ψ and its normal derivative in the regions on both sides of the node. With the help of the boundary conditions, the boundary values in the region below the node can be expressed in terms of the values for the region above the node. In a 2D scattering problem, the system of equations can be written in a matrix form as

$$M\mathbf{x} = \mathbf{y}, \tag{59}$$

where M is a $2N \times 2N$ block matrix, x is a vector of size $2N \times 1$ comprising of the values of the field and its normal derivative at the nodes, and $\mathbf{y}$ is a $2N \times 1$ vector which contains the contribution of the incident field. Once the boundary values have been solved, the field inside the boundary can be calculated from Eq. (36).

BEM resembles closely the finite-element method (FEM) [54] with the important difference that only the boundaries of homogeneous regions in the system need to be discretized. Furthermore, the finite computational domain is not a problem in BEM, e.g., the radiation condition which is satisfied by the scattered field can be directly imposed. This is a significant simplification in scattering calculations as there is no need to eliminate the influence of a finite computational domain using, for example, a perfectly matched layer as in FEM or in the finite-difference time-domain (FDTD) method [55].

The TE/TM-decomposition brings about a great computational simplification as it allows one to work with a single scalar function, but it cannot be used in dealing with a general three-dimensional (3D) scattering problem. However, the surface integral formulation of the scattering problem is also attractive for 3D problems, as the dimensionality of the problem is reduced by one and the radiation condition is taken into account automatically. There exists a variety of different forms of surface integral equations for the electric and magnetic fields [56–58]. An implementation of 3D BEM for an electromagnetic scattering problem utilizing dyadic Green's functions [58] and a direct method of integration of the strongly [59, 60] and weakly singular integrals [53] has been presented in Ref. [61].

2.5 Angular spectrum representation

A useful mathematical technique for studying wave fields in homogeneous media is the angular spectrum representation which is based on plane-wave expansions of the wave fields [24, 50]. This representation has an intuitive physical interpretation, although it is restricted to deal with fields in source-free half space or in a domain which is bounded by two mutually parallel planes [24]. The representation can be used to deal with both deterministic and random fields, and in Paper IV it is applied to propagation of the coherent modes of a random field (see Sec. 3.4). In this section, the angular spectrum representation for a monochromatic scalar field will be presented.

Consider a monochromatic wavefield

$$V(\mathbf{r}, t) = U(\mathbf{r}) \exp(-\mathrm{i}\omega t) \tag{60}$$

inside a slab D which is limited by two planes at $z = 0$ and $z \leq Z$. The slab consists of homogeneous material with refractive index $n(\omega)$ and all the sources of the field are assumed to be located outside D. The spatial part $U(\mathbf{r})$ satisfies the

Helmholtz equation (33). Assuming that in any plane with constant z inside the slab, the field can be expressed as a Fourier integral

$$U(x,y,z) = \iint_{-\infty}^{\infty} \mathcal{U}(u,v;z)\exp[\mathrm{i}(ux+vy)]\mathrm{d}u\mathrm{d}v, \tag{61}$$

it follows by inserting this into the Helmholtz equation (33) that $\mathcal{U}(u,v;z)$ satisfies

$$\frac{\partial \mathcal{U}(u,v;z)}{\partial z^2} + w^2\mathcal{U}(u,v;z) = 0, \tag{62}$$

with

$$w = \begin{cases} +(k^2-u^2-v^2)^{1/2} & \text{when} \quad u^2+v^2 \le k^2, \\ +\mathrm{i}(u^2+v^2-k^2)^{1/2} & \text{when} \quad u^2+v^2 > k^2. \end{cases} \tag{63}$$

Using the general solution of the differential equation (62), the field inside the slab can be expressed as [24]

$$\begin{aligned} U(x,y,z) \;\; = \;\; & \iint_{-\infty}^{\infty} A(u,v)\exp[\mathrm{i}(ux+vy+wz)]\mathrm{d}u\mathrm{d}v \\ & + \iint_{-\infty}^{\infty} B(u,v)\exp[\mathrm{i}(ux+vy-wz)]\mathrm{d}u\mathrm{d}v, \end{aligned} \tag{64}$$

where $A(u,v)$ and $B(u,v)$ are arbitrary functions. The result for a field which propagates into the half-space $z \ge 0$ and whose sources are located in $z < 0$, is obtained in the limit $Z \to \infty$ in which case $B(u,v)$ in Eq. (64) vanishes [24]. The angular spectrum representation for such a field consists of two kinds of plane waves [24]. The plane waves with $u^2+v^2 \le k^2$ describe homogeneous waves which propagate into the half-space $z \ge 0$. The waves with $u^2+v^2 > k^2$ are inhomogeneous waves whose amplitudes decay exponentially with increasing distance z from the plane at $z = 0$.

From the angular spectrum representation, it is seen that the spectral amplitudes $A(u,v)$ of each plane-wave component are given by the Fourier transform of the field $U_0(x,y) = U(x,y,0)$ at the plane $z = 0$:

$$A(u,v) = \tilde{U}_0(u,v). \tag{65}$$

If the field is known at the plane $z = 0$, it is known throughout the half-space $z \ge 0$ in terms of the angular spectrum representation of the field. The angular spectrum representation for electromagnetic fields can be derived in an analogous manner to the scalar case [1, 50].

3 Electromagnetic theory of optical coherence

The methods presented in the previous section deal with deterministic fields. In reality, there always exist some random fluctuations and the current and charge densities as well as the electric and magnetic fields are never strictly deterministic. In order to analyze the fluctuating electromagnetic fields, it is necessary to employ tools provided by the optical coherence theory [23–27].

In this section, the basic concepts of the second-order electromagnetic coherence theory in the space-frequency domain are introduced. In particular, the emphasis is on certain known results applicable to scalar fields and on their recent extension to arbitrary three-dimensional electromagnetic fields. The electromagnetic extension is required in order to deal with the coherence properties of, e.g., optical near-fields which are the topics of Papers I and IV. Furthermore, in Paper III the electromagnetic coherent-mode representation is explicitly derived for certain type of fluctuating fields.

3.1 Cross-spectral density tensors

The second-order coherence properties of a fluctuating electromagnetic field are characterized by the electric, magnetic, and two mixed-field coherence tensors [24]. For stationary fields the electric space-time coherence matrix is defined by the formula

$$\mathcal{E}_{jk}(\mathbf{r}_1, \mathbf{r}_2, \tau) = \langle E_j^*(\mathbf{r}_1, t) E_k(\mathbf{r}_2, t+\tau) \rangle, \tag{66}$$

where $(j,k) = (x,y,z)$ denote the Cartesian components of the electric field. The asterisk denotes complex conjugation and the angle brackets stand for ensemble averaging which for ergodic fields is equal to time averaging [24]. According to the generalized Wiener-Khintchine theorem, the electric cross-spectral density tensor and the electric coherence tensor are related to each other via [24]

$$W_{jk}^{(e)}(\mathbf{r}_1, \mathbf{r}_2, \omega) = \frac{1}{2\pi} \int_{-\infty}^{\infty} \mathcal{E}_{jk}(\mathbf{r}_1, \mathbf{r}_2, \tau) \exp(\mathrm{i}\omega\tau) \mathrm{d}\tau, \tag{67}$$

$$\mathcal{E}_{jk}(\mathbf{r}_1, \mathbf{r}_2, \tau) = \int_{0}^{\infty} W_{jk}^{(e)}(\mathbf{r}_1, \mathbf{r}_2, \omega) \exp(\mathrm{i}\omega\tau) \mathrm{d}\omega, \tag{68}$$

i.e., they form a Fourier transform pair. The lower limit in the latter integral is zero because the analytic signal representation of the fields is used [24]. Similar relations hold also for the three other cross-spectral density tensors.

The four cross-spectral density tensors may also be introduced via the Fourier

transforms of the electric and magnetic fields as [24]

$$\langle \tilde{\mathbf{E}}_j^*(\mathbf{r}_1,\omega)\tilde{\mathbf{E}}_k(\mathbf{r}_1,\omega')\rangle = W_{jk}^{(e)}(\mathbf{r}_1,\mathbf{r}_2,\omega)\delta(\omega-\omega'), \quad (69)$$

$$\langle \tilde{\mathbf{H}}_j^*(\mathbf{r}_1,\omega)\tilde{\mathbf{H}}_k(\mathbf{r}_1,\omega')\rangle = W_{jk}^{(h)}(\mathbf{r}_1,\mathbf{r}_2,\omega)\delta(\omega-\omega'), \quad (70)$$

$$\langle \tilde{\mathbf{E}}_j^*(\mathbf{r}_1,\omega)\tilde{\mathbf{H}}_k(\mathbf{r}_1,\omega')\rangle = W_{jk}^{(m)}(\mathbf{r}_1,\mathbf{r}_2,\omega)\delta(\omega-\omega'), \quad (71)$$

$$\langle \tilde{\mathbf{H}}_j^*(\mathbf{r}_1,\omega)\tilde{\mathbf{E}}_k(\mathbf{r}_1,\omega')\rangle = W_{jk}^{(n)}(\mathbf{r}_1,\mathbf{r}_2,\omega)\delta(\omega-\omega'), \quad (72)$$

where the Dirac delta function is a consequence of stationarity and shows that the different frequency components of a stationary field are uncorrelated. The four cross-spectral density tensors are not independent since they are coupled via Maxwell's equations.

The electric and magnetic cross-spectral density tensors have the property

$$\left[W_{kj}^{(e,h)}(\mathbf{r}_2,\mathbf{r}_1,\omega)\right]^* = W_{jk}^{(e,h)}(\mathbf{r}_1,\mathbf{r}_2,\omega), \quad (73)$$

and they satisfy the following non-negative definiteness condition [24]

$$\int \mathrm{d}^3 r_1 \int \mathrm{d}^3 r_2 f_j^*(\mathbf{r}_1) f_k(\mathbf{r}_2) W_{jk}^{(e,h)}(\mathbf{r}_1,\mathbf{r}_2,\omega) \geq 0, \quad (74)$$

where $f_j(\mathbf{r})$ are arbitrary well-behaved functions of position [24].

When points $\mathbf{r}_1$ and $\mathbf{r}_2$ coincide ($\mathbf{r} = \mathbf{r}_1 = \mathbf{r}_2$), the matrix $W_{jk}^{(e)}(\mathbf{r},\mathbf{r},\omega)$ forms a 3×3 Hermitian matrix called the spectral coherence matrix

$$\phi_{jk}(\mathbf{r},\omega) = W_{jk}^{(e)}(\mathbf{r},\mathbf{r},\omega), \quad (75)$$

where the diagonal elements of ϕ_{jk} are the spectral densities associated with the electric field component $E_j(\mathbf{r},\omega)$. The sum of the diagonal components, i.e., the trace (tr) of $\phi_{jk}(\mathbf{r},\omega)$, gives the total spectral density of the electric field. The off-diagonal components, $\phi_{jk}(\mathbf{r},\omega), j \neq k$, characterize the correlations between the orthogonal field components of the electric field at point $\mathbf{r}$.

For the mixed cross-spectral density tensors, the following symmetry relation holds

$$\left[W_{kj}^{(m)}(\mathbf{r}_2,\mathbf{r}_1,\omega)\right]^* = W_{jk}^{(n)}(\mathbf{r}_1,\mathbf{r}_2,\omega). \quad (76)$$

The average Poynting vector can be written in terms of the mixed cross-spectral tensors as [24]

$$\langle \mathcal{S}_k(\mathbf{r})\rangle = \frac{1}{4}\sum_{lm} \epsilon_{klm}[W_{lm}^{(m)}(\mathbf{r},\mathbf{r},\omega) - W_{lm}^{(n)}(\mathbf{r},\mathbf{r},\omega)], \quad (77)$$

where ϵ_{klm} is the Levi-Civita antisymmetric unit tensor. This form of the average Poynting vector is used in Paper IV to characterize the flow of energy in nanocylinder chains illuminated by a partially coherent field.

It has been shown that the cross-spectral density tensors are correlation tensors that can be expressed as averages over an ensemble of strictly monochromatic realizations at the same frequency [62, 63]. This property allows, for example, the electric cross-spectral density tensor to be written as an average over the ensemble $\{\mathbf{E}(\mathbf{r},\omega)\exp(\mathrm{i}\omega t)\}$ as

$$W_{jk}^{(e)}(\mathbf{r}_1,\mathbf{r}_2,\omega) = \langle E_j^*(\mathbf{r}_1,\omega)E_k(\mathbf{r}_2,\omega)\rangle, \tag{78}$$

where it should be emphasized that $E_i(\mathbf{r},\omega)$ $(i = j,k)$ is not the Fourier transform of $E_i(\mathbf{r},t)$.

In the following, quantities describing the polarization and coherence of electric fields are considered. From here onwards the superscript e is left out for brevity, and W is understood to refer to the electric cross-spectral density tensor unless otherwise stated.

3.2 Degree of polarization

Planar fields

For a planar electromagnetic field propagating in the z-direction, with the electric field oscillating in the xy-plane, the polarization statistics is described by the 2×2 spectral coherence matrix

$$\Phi_2(\mathbf{r},\omega) = \begin{pmatrix} \phi_{xx}(\mathbf{r},\omega) & \phi_{xy}(\mathbf{r},\omega) \\ \phi_{yx}(\mathbf{r},\omega) & \phi_{yy}(\mathbf{r},\omega) \end{pmatrix}. \tag{79}$$

The coherence matrix $\Phi_2(\mathbf{r},\omega)$ can be uniquely expressed as a sum of two matrices, one of which represents completely unpolarized light and is proportional to the 2×2 unit matrix, and another (Φ_2^{pol}) which represents completely polarized light. The degree of polarization of the planar field can be defined as a ratio of the spectral density of the polarized part to that of the total field [24]

$$P_2 \equiv \frac{\mathrm{tr}\Phi_2^{\mathrm{pol}}}{\mathrm{tr}\Phi_2} = \left(1 - \frac{4\det\Phi_2}{\mathrm{tr}^2\Phi_2}\right)^{1/2} = 2\left\{\frac{\mathrm{tr}\left[\Phi_2^2(\mathbf{r},\omega)\right]}{\mathrm{tr}^2\left[\Phi_2(\mathbf{r},\omega)\right]} - \frac{1}{2}\right\}^{1/2}. \tag{80}$$

The degree of polarization, P_2, is bounded to the interval $0 \le P_2(\mathbf{r},\omega) \le 1$ with $P_2 = 1$ corresponding to a completely polarized and $P_2 = 0$ to a completely unpolarized plane wave.

Alternatively, the degree of polarization can be described in terms of the four Stokes parameters [24, 27]

$$\begin{aligned} S_0(\mathbf{r},\omega) &= \phi_{xx}(\mathbf{r},\omega) + \phi_{yy}(\mathbf{r},\omega), && (81)\\ S_1(\mathbf{r},\omega) &= \phi_{xx}(\mathbf{r},\omega) - \phi_{yy}(\mathbf{r},\omega), && (82)\\ S_2(\mathbf{r},\omega) &= \phi_{xy}(\mathbf{r},\omega) + \phi_{yx}(\mathbf{r},\omega), && (83)\\ S_3(\mathbf{r},\omega) &= \mathrm{i}\left[\phi_{yx}(\mathbf{r},\omega) - \phi_{xy}(\mathbf{r},\omega)\right]. && (84) \end{aligned}$$

The parameter $S_0(\mathbf{r},\omega)$, gives the spectral density of the field. The parameter $S_1(\mathbf{r},\omega)$ describes the excess in spectral density of the x component over that of the y component of the field. The parameter $S_2(\mathbf{r},\omega)$ represents the excess of $+45^\circ$ linearly polarized component over -45° linearly polarized component, and $S_3(\mathbf{r},\omega)$ the excess in the spectral density of the right-hand circularly polarized field component over the left-hand circularly polarized one [23, 27].

The Stokes parameters appear as expansion coefficients when the coherence matrix is expanded in terms of the 2×2 unit matrix σ_0 and the three Pauli matrices σ_j $(j = 1, 2, 3)$ as

$$\Phi_2(\mathbf{r},\omega) = \frac{1}{2}\sum_{j=0}^{3} S_j(\mathbf{r},\omega)\sigma_j. \qquad (85)$$

Inserting this expansion into Eq. (80) gives the degree of polarization in terms of the four Stokes parameters as [24, 27]

$$P_2(\mathbf{r},\omega) = \frac{\left[S_1^2(\mathbf{r},\omega) + S_2^2(\mathbf{r},\omega) + S_3^2(\mathbf{r},\omega)\right]^{1/2}}{S_0(\mathbf{r},\omega)}. \qquad (86)$$

Non-planar fields

Next the extension of the previous formalism to arbitrary three-dimensional (non-planar) fields [64, 65] will be considered . For such a field the 3×3 spectral coherence matrix is

$$\Phi_3(\mathbf{r},\omega) = \begin{pmatrix} \phi_{xx}(\mathbf{r},\omega) & \phi_{xy}(\mathbf{r},\omega) & \phi_{xz}(\mathbf{r},\omega) \\ \phi_{yx}(\mathbf{r},\omega) & \phi_{yy}(\mathbf{r},\omega) & \phi_{yz}(\mathbf{r},\omega) \\ \phi_{zx}(\mathbf{r},\omega) & \phi_{zy}(\mathbf{r},\omega) & \phi_{zz}(\mathbf{r},\omega) \end{pmatrix}. \qquad (87)$$

Unlike in the case of planar fields, Φ_3 cannot generally be expressed as a sum of a completely unpolarized (proportional to 3×3 unit matrix) and completely polarized part. However, the generalization of the degree of polarization to non-planar field can be obtained by considering the expansion of Φ_3 in terms of proper basis matrices. This is the approach taken by Setälä *et al.* in Refs. [64, 65] where the 3×3 unit

matrix λ_0 and the eight Gell-Mann matrices λ_j ($j = 1, \ldots, 8$) are used as basis. In this basis the coherence matrix is written as [27, 64]

$$\Phi_3(\mathbf{r}, \omega) = \frac{1}{3} \sum_{j=0}^{8} \Lambda_j(\mathbf{r}, \omega) \lambda_j, \tag{88}$$

where the nine expansion coefficients Λ_j are called 3D (spectral) Stokes parameters [64]. The degree of polarization, P_3, of an arbitrary 3D electromagnetic field is defined by the formula [22, 64] (see also [66, 67])

$$P_3^2(\mathbf{r}, \omega) = \frac{1}{3} \frac{\sum_{j=1}^{8} \Lambda_j^2(\mathbf{r}, \omega)}{\Lambda_0^2(\mathbf{r}, \omega)} = \frac{3}{2} \left\{ \frac{\mathrm{tr}\left[\Phi_3^2(\mathbf{r}, \omega)\right]}{\mathrm{tr}^2\left[\Phi_3(\mathbf{r}, \omega)\right]} - \frac{1}{3} \right\}. \tag{89}$$

More recently, the same form has also been put forward by Luis, who has formulated the degree of polarization as a distance between the coherence matrix of the field and the identity matrix representing completely unpolarized 3D light [68]. The physical meaning of P_3 becomes transparent by writing it in a coordinate system which is oriented in such a way that $\phi_{xx}(\mathbf{r}, \omega) = \phi_{yy}(\mathbf{r}, \omega) = \phi_{zz}(\mathbf{r}, \omega)$. Such an orientation can always be found [64]. In this specific coordinate system P_3^2 has the form [64, 65]

$$P_3^2(\mathbf{r}, \omega) = \frac{|\mu_{xy}(\mathbf{r}, \omega)|^2 + |\mu_{xz}(\mathbf{r}, \omega)|^2 + |\mu_{yz}(\mathbf{r}, \omega)|^2}{3}, \tag{90}$$

where the quantities

$$\mu_{jk}(\mathbf{r}, \omega) = \frac{\phi_{jk}(\mathbf{r}, \omega)}{[\phi_{jj}(\mathbf{r}, \omega)\phi_{kk}(\mathbf{r}, \omega)]^{1/2}} \tag{91}$$

are the normalized off-diagonal elements of the coherence matrix. The 3D degree of polarization is seen to be a measure for the average correlations between the three orthogonal electric field components.

The value of P_3 is bounded to the interval $0 \leq P_3 \leq 1$ like P_2 [64]. It is also invariant under unitary operations, e.g., rotations of coordinates system, since these do not change the value of trace. However, the 2D and 3D formalisms do not, in general, give the same value for the degree of polarization of a planar field [64]. For such a field, the 3D degree of polarization is restricted to the values $0.5 \leq P_3 \leq 1$ with the value $P_3 = 1/2$ corresponding to a plane wave which in 2D sense is completely unpolarized ($P_2 = 0$). The dependence of the value of the degree of polarization on the dimensionality of the problem has been studied in connection with intensity correlations of fields obeying Gaussian statistics [69].

There has recently been an extensive discussion in the literature on the extension of the degree of polarization to non-planar fields, and some other definitions for the

degree of polarization have also been proposed (for review, see [70]). Besides considerations based on classical coherence theory, the degree of polarization for 3D quantum light fields based on Stokes parameters, which in quantum optics are represented by Stokes operators, has also been put forward [71]. In the quantum domain the polarization is fundamentally a 3D phenomenon as it involves the fluctuations of all three field components even in the vacuum state [71]. However, the adequacy of the Stokes parameters that characterize only the second-order correlations of the field amplitudes, has been questioned for describing quantum fields [72]. For these fields, higher-order correlations are also important, and the Stokes parameters do not necessarily distinguish quantum states even though they have significantly different polarization properties. In particular, the degree of polarization (2D) can be zero for field states that cannot be considered as unpolarized [73]. The 3D degree of polarization presented in Eq. (89) is adequate for describing classical non-planar fields such as optical near-fields [22] which are also studied in Papers I and IV, or tightly focused beams [74, 75].

3.3 Electromagnetic degree of coherence

In scalar theory, the spectral degree of coherence $|\mu(\mathbf{r}_1, \mathbf{r}_2, \omega)|$, which characterizes at angular frequency ω the second-order field correlations at points $\mathbf{r}_1$ and $\mathbf{r}_2$, is given by [24]

$$|\mu(\mathbf{r}_1, \mathbf{r}_2, \omega)| = \frac{|W(\mathbf{r}_1, \mathbf{r}_2, \omega)|}{[S(\mathbf{r}_1, \omega) S(\mathbf{r}_2, \omega)]^{1/2}}. \tag{92}$$

Here $W(\mathbf{r}_1, \mathbf{r}_2, \omega)$ is the cross-spectral density and $S(\mathbf{r}_j, \omega) = W(\mathbf{r}_j, \mathbf{r}_j, \omega)$ ($j = 1, 2$) is the spectral density. The values of the spectral degree of coherence are limited to $0 \leq |\mu(\mathbf{r}_1, \mathbf{r}_2, \omega)| \leq 1$ with the upper bound corresponding to a spatially fully coherent field. For such a field the cross-spectral density has a factorized form in the spatial coordinates $\mathbf{r}_1$ and $\mathbf{r}_2$ [24]. Furthermore, when $\mathbf{r}_1$ and $\mathbf{r}_2$ coincide, spectral degree of coherence has the value $|\mu(\mathbf{r}, \mathbf{r}, \omega)| = 1$. The spectral degree of coherence in the context of scalar fields, describes under suitable conditions, the visibility of intensity fringes in the classical Young's two-pinhole experiment [24].

The generalization of the spectral degree of coherence to electromagnetic fields has been proposed, akin to the scalar case, by considering the visibility of interference fringes in Young's experiment [76, 77]. However, there are some problems with this definition [78, 80–84] which have lead to an alternative definition of the spectral degree of coherence for electromagnetic fields [78–80] as

$$\zeta(\mathbf{r}_1, \mathbf{r}_2, \omega) = \frac{\| \overleftrightarrow{W}(\mathbf{r}_1, \mathbf{r}_2, \omega) \|_{\mathrm{F}}}{\left[\mathrm{tr}\ \overleftrightarrow{W}(\mathbf{r}_1, \mathbf{r}_1, \omega)\right]^{1/2} \left[\mathrm{tr}\ \overleftrightarrow{W}(\mathbf{r}_2, \mathbf{r}_2, \omega)\right]^{1/2}}. \tag{93}$$

In this equation

$$\begin{aligned} \| \overleftrightarrow{W}(\mathbf{r}_1, \mathbf{r}_2, \omega)\|_{\mathrm{F}} &= \mathrm{tr}\left[\overleftrightarrow{W}(\mathbf{r}_1, \mathbf{r}_2, \omega) \cdot \overleftrightarrow{W}^{\dagger}(\mathbf{r}_1, \mathbf{r}_2, \omega)\right]^{1/2} \\ &= \Big[\sum_{i,j} |W_{ij}(\mathbf{r}_1, \mathbf{r}_2, \omega)|^2 \Big]^{1/2}, \end{aligned} \tag{94}$$

denotes the Frobenius norm and the dagger stands for the Hermitian adjoint. Recently it has been shown that the electromagnetic degree of coherence ζ is a measure of both the visibility of the intensity fringes (modulation in the Stokes parameter S_0) and the modulation contrasts of the three polarization Stokes parameters (S_1, S_2, S_3) in Young's double-slit interference experiment [85, 86]. The quantity $\zeta(\mathbf{r}_1, \mathbf{r}_2, \omega)$ is real and limited to the values $0 \leq \zeta(\mathbf{r}_1, \mathbf{r}_2, \omega) \leq 1$ like its scalar counterpart $|\mu(\mathbf{r}_1, \mathbf{r}_2, \omega)|$. In fact, for uniformly polarized waves, $\zeta(\mathbf{r}_1, \mathbf{r}_2, \omega)$ reduces to the spectral degree of coherence $|\mu(\mathbf{r}_1, \mathbf{r}_2, \omega)|$ for scalar waves. Furthermore, like in the scalar case, the cross-spectral density tensor factors in its two spatial variables if and only if $\zeta(\mathbf{r}_1, \mathbf{r}_2, \omega) = 1$. The factorization property can be considered to be a fundamental property of a completely coherent field [87]. The definition of Eq. (93) is applicable for scalar fields, electromagnetic beams as well as for arbitrary 3D fields which are encountered in near-field optics.

For electromagnetic fields, the quantity $\zeta(\mathbf{r}_1, \mathbf{r}_2, \omega)$, when evaluated for $\mathbf{r} = \mathbf{r}_1 = \mathbf{r}_2$, is related to the degree of polarization, in the case of 2D beams, as

$$\zeta(\mathbf{r}, \mathbf{r}, \omega) = [(P_2^2(\mathbf{r}, \omega) + 1)/2]^{1/2} \tag{95}$$

and as

$$\zeta(\mathbf{r}, \mathbf{r}, \omega) = [(2P_3^2(\mathbf{r}, \omega) + 1)/3]^{1/2}, \tag{96}$$

in the case of 3D fields. Thus, in the electromagnetic case, the equal-point degree of correlations equals unity if and only if the field is completely polarized [78, 80].

3.4 Coherent-mode representation

The coherent-mode representation of scalar fields [62] is an important tool that has been applied to a number of radiation and propagation, and scattering problems. In this section a brief summary of the basic concepts pertaining to the coherent-mode representation of fluctuating, statistically stationary scalar fields [24] and the extension of the representation to full vector fields [63, 88] is presented.

Scalar fields

At any frequency ω, the coherence properties of the field at two points in space, $\mathbf{r}_1$ and $\mathbf{r}_2$, are described by the cross-spectral density function, defined by the Fourier

transform

$$W(\mathbf{r}_1, \mathbf{r}_2, \omega) = \frac{1}{2\pi} \int_{-\infty}^{\infty} \Gamma(\mathbf{r}_1, \mathbf{r}_2, \tau) \exp(\mathrm{i}\omega\tau) \mathrm{d}\tau, \tag{97}$$

where

$$\Gamma(\mathbf{r}_1, \mathbf{r}_2, \tau) = \langle U^*(\mathbf{r}_1, t) U(\mathbf{r}_2, t+\tau) \rangle \tag{98}$$

is the mutual coherence function. The function $U(\mathbf{r}, t)$ is the complex analytic signal associated with the random scalar field and the mutual coherence function $\Gamma(\mathbf{r}_1, \mathbf{r}_2, \tau)$ characterizes the field correlations between the two points at time difference τ. The scalar cross-spectral density functions are Hermitian and non-negative definite Hilbert-Schmidt kernels, and therefore they admit the following Mercer series representation [24]

$$W(\mathbf{r}_1, \mathbf{r}_2, \omega) = \sum_n \alpha_n(\omega) \psi_n^*(\mathbf{r}_1, \omega) \psi_n(\mathbf{r}_2, \omega). \tag{99}$$

The quantities $\alpha_n(\omega)$ and $\psi_n(\mathbf{r}, \omega)$ are the eigenvalues and eigenfunctions, respectively, of a homogeneous Fredholm integral equation of the second kind

$$\int_D W(\mathbf{r}_1, \mathbf{r}_2, \omega) \psi_n(\mathbf{r}_1, \omega) \mathrm{d}^3 r_1 = \alpha_n(\omega) \psi_n(\mathbf{r}_2, \omega), \tag{100}$$

where the integration is performed over the domain D. By defining the inner product of two functions $a(\mathbf{r})$ and $b(\mathbf{r})$ over D to be

$$\{a(\mathbf{r}), b(\mathbf{r})\}_D \equiv \int_D a^*(\mathbf{r}) b(\mathbf{r}) \mathrm{d}^3 r, \tag{101}$$

the set of eigenfunctions can be chosen to be orthonormal, i.e.,

$$\{\psi_m(\mathbf{r}, \omega), \psi_n(\mathbf{r}, \omega)\}_D = \delta_{mn}, \tag{102}$$

where δ_{mn} is the Kronecker delta. The factors $\psi_n(\mathbf{r}, \omega)$ satisfy the Helmholtz equation, and thus each term in the summation in Eq. (99) likewise obeys a pair of Helmholtz equations. Since the terms in the summation are of a spatially factored form, they represent elementary modes which are completely coherent, and therefore, Eq. (99) is called the coherent-mode representation of the cross-spectral density function [24, 62].

Electromagnetic fields

The extension of the coherent-mode decomposition to partially polarized paraxial [88] and full three-dimensional vector fields [63] has recently been introduced. The coherent-mode representation of electromagnetic fields is constructed in analog to

that of scalar fields. The electric cross-spectral density tensor, which satisfies the specific Hermiticity, non-negative definiteness, and square-integrability conditions, can be expanded as a Mercer series of the form [63, 88]

$$\overleftrightarrow{W}\,(\mathbf{r}_1, \mathbf{r}_2, \omega) = \sum_n \lambda_n(\omega) \boldsymbol{\psi}_n^*(\mathbf{r}_1, \omega) \boldsymbol{\psi}_n(\mathbf{r}_2, \omega), \qquad \mathbf{r}_1, \mathbf{r}_2 \in D, \tag{103}$$

when the inner product for vector-valued complex functions in the volume D is defined to be

$$\{\mathbf{A}(\mathbf{r}), \mathbf{B}(\mathbf{r})\}_D \equiv \int_D \mathbf{A}^*(\mathbf{r}) \cdot \mathbf{B}(\mathbf{r})\, \mathrm{d}^3 r. \tag{104}$$

In Eq. (103) the quantities $\lambda_n(\omega)$ and $\boldsymbol{\psi}_n(\mathbf{r}, \omega)$ are the eigenvalues and vector-valued eigenfunctions, respectively, of the homogeneous Fredholm integral equation of the second kind

$$\int_D \boldsymbol{\psi}_n(\mathbf{r}_1, \omega) \cdot \overleftrightarrow{W}\,(\mathbf{r}_1, \mathbf{r}_2, \omega) \mathrm{d}^3 r_1 = \lambda_n(\omega) \boldsymbol{\psi}_n(\mathbf{r}_2, \omega). \tag{105}$$

The eigenvalues are real and non-negative, and the eigenfunctions form an orthonormal set in the sense that

$$\{\boldsymbol{\psi}_n(\mathbf{r}, \omega), \boldsymbol{\psi}_m(\mathbf{r}, \omega)\}_D = \delta_{nm}. \tag{106}$$

Although the orthogonality does not automatically hold if an eigenvalue is degenerate, the corresponding eigenfunctions can always be made orthogonal.

It can be shown that the factors $\boldsymbol{\psi}_n(\mathbf{r}, \omega)$ and the tensors

$$\overleftrightarrow{W}_n\,(\mathbf{r}_1, \mathbf{r}_2, \omega) = \lambda_n(\omega) \boldsymbol{\psi}_n^*(\mathbf{r}_1, \omega) \boldsymbol{\psi}_n(\mathbf{r}_2, \omega) \tag{107}$$

satisfy the appropriate Helmholtz equations and Maxwell's divergence conditions [78]. In addition, since the tensors $\overleftrightarrow{W}_n\,(\mathbf{r}_1, \mathbf{r}_2, \omega)$ are of a spatially factored form, they may be understood as elementary cross-spectral density tensors representing completely coherent (and completely polarized [64]) electric fields in the space–frequency domain [79], in the sense of the definition of the spectral degree of coherence for electromagnetic fields in Eq. (93).

The coherent-mode representation has mainly been applied to two-dimensional (or beam-like) scalar fields with a few exceptions [89,90] in which the vector nature of the field is considered. In particular, the coherent-mode representation for electromagnetic Gaussian Schell-model beams has previously been utilized [78, 91]. In paper III an explicit three-dimensional coherent-mode representation, the first and only so far, is derived for both scalar and electromagnetic fields. The representation in Paper III applies to electromagnetic fields whose electric cross-spectral density tensor is proportional to the imaginary part of the infinite-space Green tensor. It is

known that fields generated by statistically stationary, homogeneous, and isotropic source distributions, in an unbounded low-loss medium have this property. The analysis covers the fundamental case of black-body radiation, but it is also valid more generally; since a thermal equilibrium condition is not invoked, the electromagnetic field may have any spectral distribution. The theory is useful for the analysis of optical coherence in a wide variety of 3D situations, e.g., in light scattering from (nano)particles, general electromagnetic near fields, and tightly focused fields. The coherent-mode representation can significantly simplify the analysis of optical systems for partially coherent light. Instead of the two-point correlation functions, only the coherent modes, which depend on a single spatial variable, need to be studied in propagation through the optical system. Furthermore, the analytical form of the coherent modes is only rarely known, and hence the exact representation in Paper III is a valuable addition to the existing literature.

4 Electromagnetic fields in nanostructures

In this section certain specific physical phenomena of near field optics are considered: the scanning near-field optical microscopy (SNOM), enhanced optical transmission through a sub-wavelength slit, plasmon resonances in metallic nanoparticles and nanowires, as well as the radiative properties and energy transfer of molecular systems in complex environments. These are the subjects of Papers I, II, IV, and V where the theoretical methods presented in the previous two sections are applied.

4.1 Scanning near-field optical microscopy

In conventional (far-field) microscopy the best obtainable resolution is on the order of the wavelength of light [23]. The resolution can be slightly enhanced, for example, by using a solid immersion lens to increase the numerical aperture of the imaging system [1]. However, these conventional means of imaging are inadequate to acquire sub-wavelength-scale optical information about nanostructures which is of interest in nano-optics. From the angular spectrum representation of optical fields (see Sec. 2.5), it can be seen that the information about the sub-wavelength features of the sample are contained in the high spatial-frequency components of the field which decay exponentially away from the sample [92]. The free-space propagation of the field acts as a low-pass filter and hence these evanescent (non-radiative) components are not detected in the far zone [50]. To obtain optical information about the sub-wavelength features of the sample it is necessary to extract information contained in the evanescent components which are strong only within the distance of the wavelength of light from the surface of an emitting or scattering object. This is achieved in scanning near-field optical microscopy (SNOM) [3–6] where the basic idea is to use a nanoprobe to detect the evanescent field above the sample surface. The nanoprobe scatters some of the evanescent field components into propagating waves that can be detected in the far zone by conventional means. By scanning the nanoprobe over the sample surface, the evanescent field distribution can be mapped with a resolution limited mainly by the size of the nanoprobe and the scanning height. In practice, the resolution achieved in a near-field measurement is on the order of tens of nanometers providing an improvement by an order of magnitude to the best conventional far-zone measurements. Optical near-field microscopy has become one of the standard techniques among the scanning-probe microscopies and is an important tool in nano-optics at present.

There exist several operation modes in SNOM depending on whether the probe is used as a local illuminator, local collector, or for both purposes. From a theoretical point of view it is often enough to analyze the probe in only one mode of operation as the reciprocity theorem of electromagnetism states that a signal remains unchanged upon exchange of source and detector [1, 7]. A wide variety of nanoprobes

has been utilized in SNOM measurements [1]. The most typical nanoprobe, the so-called aperture probe, is a metal-coated, tapered optical fiber with a nanoaperture at the apex [8]. The purpose of the metal coating is to confine the field inside the fiber and thus obtain a very localized field at the probe apex. Due to the finite skin depth of metals the field penetrates also some distance into the metal cladding hence increasing the attainable spot size at the aperture. Aluminum is most often used for coating as it has small skin depth. Also uncoated dielectric probes are common. Whereas low throughput can be a problem in the aperture probes, the uncoated dielectric probes show low field confinement [1]. Another important class of probes is the apertureless probes such as pointed metal tips and small metal particles where strong local field enhancement can be achieved [1]. Also nanoemitters, such as single molecules or nanocrystals have been employed in SNOM measurements [1]. The resolution which can be achieved in a SNOM measurement depends not only on the properties of the nanoprobe, but also on the properties of the sample. Considerable amount of attention has been paid to investigating the interaction of the scanning probe and the sample and the image formation in near field optics [7]. It has been shown that the same object can generate completely different images when the illumination conditions, such as coherence, polarization and angle of incidence, are changed [93], and that for inhomogeneous dielectric samples, the near-field signal depends on both the topography and the dielectric contrast of the sample [94].

Theoretical modeling of SNOM

A careful modelling of the near field and the sample-probe interaction in particular, requires the full electromagnetic nature of the problem to be considered. Approximative methods such as Fresnel-Kirchhoff diffraction theory fail to accurately model SNOM, where one deals with fields in the vicinity of sub-wavelength scale objects. On the other hand, the electrostatic approximation, which is applicable at length scales smaller than the wavelength, cannot usually be exploited either, since in many cases the signal to be measured is in the far zone at a distance of several wavelengths from the sample. Realistic simulations of the SNOM probe require that the sample-probe system is treated self-consistently, i.e., the probe and the sample are considered as a single system consisting of two interacting parts. Several theoretical methods have been employed to model the electromagnetic field in SNOM [95, 96]. For example, the traditional Bethe-Bouwkamp model has been used to describe the transmission of light through the SNOM aperture [97] and the resolution limit of SNOM has been considered by means of a transfer function [98]. The multiple-multipole method (MMP) [99, 100] and FDTD method [101, 102], and boundary-integral method [47–49] have been used in analysis of the SNOM tip. Moreover, the Green's propagator formalism (volume integral method) has also

been widely employed in studies of optical near fields [94, 103–105]. In modelling apertureless probes and determining the optimal tip shape for field enhancement, antenna theory, developed originally for the radio- and microwave-frequency range, has been utilized [106].

Polarization properties of SNOM probes

The polarization properties of SNOM probes have been the subject of several recent experimental and theoretical investigations [107–110]. Not only the coupling to a fiber probe is sensitive to polarization of the electromagnetic field, but also the resolution obtainable with certain SNOM probes is highly dependent on the polarization characteristics of the optical field [108, 110]. Theoretical analyses have been concentrated on deterministic fields, but a two-dimensional analysis of light transmission through a metal-coated SNOM tip has also been carried out for partially polarized light [Paper I], in which the dependence of the degree of polarization on the opening angle and the aperture size of the tip have been analyzed. Even though the simulation is based on a 2D model of a SNOM aperture probe which has different modal properties than 3D probes, the results show that the polarization properties of the transmitted field illuminating the sample can differ significantly from the incident field which is originally coupled into the fiber. This is due to the higher transmission of TM-polarized light as compared to that of TE-polarized light through the tip. For instance, a probe with a small opening angle and a small aperture acts like a polarizer blocking the TE component and thus resulting in a high degree of polarization for the transmitted field. This is illustrated in Fig. 1 where the 3D degree of polarization is shown on a semicircle at a distance $r = 10\ \mu$m from the output aperture of an aluminium-coated, tapered SNOM probe which is illuminated by unpolarized light having wavelength $\lambda = 488$ nm [Paper I]. The output aperture has a width of 50 nm and the opening angles of the probe vary from $\alpha = 20^\circ$ to $\alpha = 45^\circ$. The characterization of the electric field correlations in the vicinity of the probe requires the use of 3D formalism for calculating the degree of polarization (P_3). Far from the probe, the transmitted field is transverse and 2D degree of polarization, P_2, can also be used. The degrees of polarization, P_2 and P_3, were shown in Paper I to provide similar information about the polarization properties of the far field although they differ in their numerical values (see Sec. 3.2). However, the use of P_3 allows a direct comparison between the near and far field polarization characteristics.

4.2 Enhanced optical transmission

After the initial demonstration of enhanced optical transmission through a periodic array of sub-wavelength holes in a metallic film [111] there has been extensive

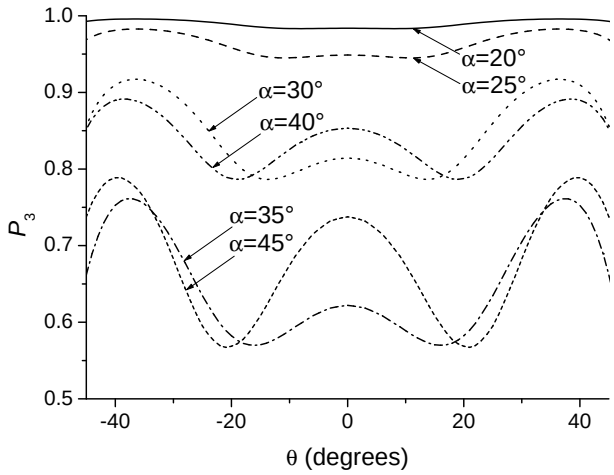

Figure 1: The angular behavior of the 3D degree of polarization, P_3, at the distance $r = 10$ μm from the output aperture of a SNOM probe. The incident wave has wavelength $\lambda = 488$ nm and is fully unpolarized. The different curves correspond to varying opening angles of the tip. The relatively high degree of polarization is attributed to the much higher transmission of TM-polarized light in comparison to TE-polarized light. [Paper I]

research on the optical properties of nanostructured metal films. The transmission through the holes can be much higher than expected from diffraction theory (Bethe-Bouwkamp model) and even exceed the percentage area occupied by the holes [111]. The transmission spectrum of a hole array shows a peak whose position can be changed by altering the periodicity and symmetry of the structure [11]. The enhanced transmission has been attributed to surface-plasmon polaritons [112–117], but for slit arrays the waveguide mode resonances also play a role [113, 117–121]. Furthermore, the enhanced transmission has been studied within the framework of dynamical diffraction theory [122, 123].

Surface plasmon polaritons

Surface plasmon polaritons are electromagnetic surface waves that can propagate along a metal-dielectric interface [9–12]. They are constituted by a resonant interaction of the electromagnetic field with the collective charge oscillations in the metal. The electric field of the wave decays exponentially away from the interface and is polarized in the plane spanned by the direction of propagation and the surface normal. On a planar interface the dispersion relation, i.e., the functional relationship between the wavenumber k_{sp} of the surface plasmon polariton and its frequency ω, is obtained from the solution to Maxwell's equations in each medium

and the boundary conditions as [11, 12]

$$k_{sp} = \frac{\omega}{c}\left[\frac{\epsilon_1(\omega)\epsilon_2}{\epsilon_1(\omega)+\epsilon_2}\right]^{1/2}, \tag{108}$$

where $\epsilon_1(\omega)$ and ϵ_2 are the (relative) permittivities of the the metal and the dielectric, respectively. The permittivity of the dielectric material depends usually only weakly on the frequency and can be assumed to be constant [1]. The momentum of the surface plasmon polariton along the metal-dielectric interface, k_{sp}, is greater than the momentum of propagating light having the same frequency [11]. This means that on a planar interface the surface plasmon polariton cannot transform into radiation, and vice versa, it cannot be excited on a planar interface by using conventional (far field) illumination. However, in the case of periodically structured metal films, the wave vectors for the propagating light and the surface plasmon polariton can be matched thus allowing a direct excitation of surface plasmon polaritons on the film [12]. Surface plasmons enhance the evanescent waves that tunnel through the holes and thus increase the transmittance [11]. Also for thin enough films surface plasmons on opposite surfaces of the film can interact resulting in a resonant tunneling effect [11]. It is thus possible to have enhanced transmission even through a film without holes [124].

Transmission through a single slit

The enhanced transmission can occur also for single slit and hole structures [125–131]. The hole and slit structures differ fundamentally in their transmission characteristics [114] as the sub-wavelength holes do not support any propagating modes whereas for slits the lowest TM mode, exhibiting surface-wave-like behavior [132], has no cutoff. In the case of a single slit the resonant transmission of light has been connected to Fabry-Pérot-like resonances [125, 127, 128]. The waveguide mode is reflected at both ends of the slit and thus the slit acts like a resonator. For periodic slit structures both the slit modes and the modes due to the periodic surface structure affect the transmission [12]. The directionality of the transmitted light can be modified by nanostructuring the metal film [129], and thus it is possible to generate a well-directed source of light emitted from the sub-wavelength aperture [133, 134]. The spectral properties of resonant transmission of light through a single sub-wavelength slit in a metal film have been analyzed by characterizing the effect of geometrical and material properties of the slit on the transmission spectrum. In particular, the resonance wavelength has been shown to depend strongly on the material within the slit [Paper II]. This is depicted in Fig. 2, where the calculated transmittance spectra of a 15 nm wide slit in a gold film with a thickness of 200 nm are presented for different materials in the slit. The shift of the resonance

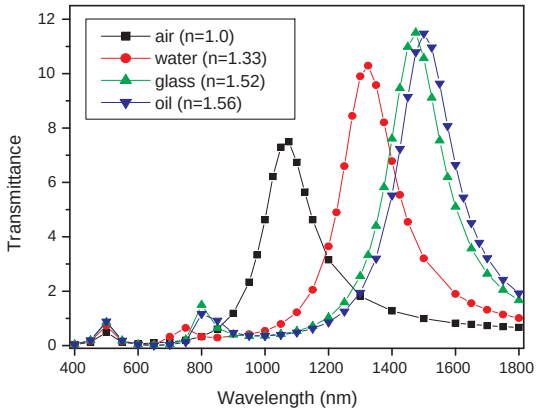

Figure 2: Transmittance spectra for a 15 nm wide slit in a 200 nm thick gold film as the material within the slit is varied. As the refractive index of the slit medium increases, the resonance peak shifts to longer wavelengths. [Paper II]

peak in the transmission spectrum is suggested to be used to detect small changes in the refractive index of the medium in the slit or in its immediate vicinity.

4.3 Plasmon resonances in metal nanoparticles

Electromagnetic surface excitations in bounded geometries are called localized surface plasmons [12]. Frequencies at which these surface plasmon resonances occur can be found in the quasi-static approximation which amounts to solving Laplace's equation [1]. The quasi-static approximation neglects the retardation effects, i.e., the speed of light is assumed to become infinitely large, and it is valid for systems whose dimensions are much smaller than the wavelength of light. In fact, since the quasi-static approximation leads to fields which are constant inside the particles, it can be considered to be valid only for particles that are smaller in size than the skin depth d of the metal, $d = \lambda/(4\pi\sqrt{\epsilon_m})$, with ϵ_m being the relative permittivity of the metal [1]. The plasmon resonances occurring in metal nanoparticles and nanowires are of particular interest in nano-optics as at the resonance wavelength the field can be locally significantly enhanced. Furthermore, the scattering cross-section can become very large at the resonance.

For 2D problems the plasmon resonances occur only for TM-polarized light as the electric field needs to have a component in the direction normal to the surface in order to drive polarization charges to the interface [1]. The (relative) permittivity of the dielectric material, ϵ_2, can often be assumed to be constant and real whereas

the metal's dielectric function ϵ_1 is strongly frequency dependent and complex. In the quasi-static approximation for a thin, metallic, cylindrical wire with radius a, the resonance condition is given by $\mathrm{Re}\{\epsilon_1(\omega)\} = -\epsilon_2$ [1]. For a spherical particle of radius a, the resonance condition can be seen from the expression for the quasi-static polarizability of the particle, which is [1]

$$\alpha_0(\omega) = 4\pi a^3 \frac{\epsilon_1(\omega) - \epsilon_2}{\epsilon_1(\omega) + 2\epsilon_2}. \tag{109}$$

For a sphere the resonance occurs when $\mathrm{Re}\{\epsilon_1(\omega)\} = -2\epsilon_2$. The resonance frequency is seen to be sensitive to the medium where the wire or particle is embedded.

To go beyond the quasi-static approximation, which is necessary, for example, in the case of larger particles or for modeling an array of particles, requires the solution to Helmholtz equation. Spherical particles that are much smaller than the wavelength of light can be approximated as point dipoles with a polarizability of a sphere. However, the expression for the polarizability must be modified from the quasi-static expression as it violates the optical theorem in the dipole limit; the extinct power is in this case identical with the absorbed energy and hence the light scattering is not taken into account [1]. This problem is solved by including the interaction of the particle with itself (radiation reaction) in the expression of the polarizability [1]. The analytical solutions to light scattering problems from a single sphere or cylinder are known [37], but for more complicated particle shapes, and in particular, for modeling interaction of several particles, a numerical solution to the scattering problem is required. The resonances in nanowires have been calculated using the volume integral method [135, 136], FDTD [137] and BEM [138–140]. Whereas for a single cylindrical nanowire there exists only one plasmon resonance, more complicated particle shapes and interacting structures exhibit much richer resonance spectra. Furthermore, the field enhancement in these structures can be orders of magnitudes higher than for a single wire with cylindrical cross-section. Currently, there is considerable interest in studies of nanoparticle chains [141–145] and nanowires [137, 146–148], as these systems can act as near-field waveguides enabling light guiding at sub-wavelength scales. Such structures could be used, for example, to transfer energy between two distant quantum systems such as molecules or quantum dots, as well as in addressing single nano-objects [149, 150].

The effect of plasmon resonances to the near field coherence properties of nanowires was analyzed in terms of the 3D degree of polarization and on the electromagnetic degree of coherence in Paper IV. The numerical calculations were based on BEM discussed in Sec. 2.4. The results show that the plasmon resonances may significantly affect the coherence and polarization characteristics of the near field of nanowire structures. Furthermore, it was demonstrated that partial coherence can influence the excitation of collective modes of nanocylinder arrays and affect also the energy flow in these arrays.

4.4 Molecules in nanostructures

Since Purcell's pioneering work [151] in 1946, which showed that the spontaneous emission is not an intrinsic property of atoms or molecules but depends on their environment, changes in the excited-state lifetimes and radiative shifts in spontaneous emission have been extensively investigated both theoretically and experimentally in various environments [16–18]. In particular, the tailoring of the radiative properties of molecules by modifying their environment offers exciting possibilities for nanophotonics applications.

Radiative decay rate

The environment induced changes in the spontaneous emission rate of a molecule or an atom can be obtained within the framework of classical electromagnetic theory by considering an oscillating dipole and its interaction with its own field which is scattered back from the environment [1, 16]. The decay rate b and the free-space decay rate b_0 can be obtained from the Green's function of the system. It is convenient to write the total Green's tensor as a sum of the free-space part $\overleftrightarrow{G}_0$ and the scattered part $\overleftrightarrow{G}_s$:

$$\overleftrightarrow{G}\left(\mathbf{r}_1, \mathbf{r}_2, \omega\right) = \overleftrightarrow{G}_0\left(\mathbf{r}_1, \mathbf{r}_2, \omega\right) + \overleftrightarrow{G}_s\left(\mathbf{r}_1, \mathbf{r}_2, \omega\right). \tag{110}$$

The free-space part is singular at $\mathbf{r}_1 = \mathbf{r}_2$ whereas the scattered part remains finite. The ratio of the decay rates is determined by the scattered part $\overleftrightarrow{G}_s$, and is given by [16]

$$\frac{b}{b_0} = 1 + \mu_0 \omega^3 \frac{Q}{b_0} \mathrm{Im}\left\{\boldsymbol{\mu} \cdot \overleftrightarrow{G}_s\left(\mathbf{r}, \mathbf{r}, \omega\right) \cdot \boldsymbol{\mu}\right\}, \tag{111}$$

where Q is the emission quantum efficiency and $\boldsymbol{\mu}$ is the dipole transition moment. The environment causes also a change in the frequency of the emitted light. However, this effect is very small and can usually be ignored [1].

Dipole-dipole interaction

The environment has an effect also on the interactions between the molecules. The dipole-dipole coupling between two molecules or atoms has been studied in microcavities [152–157], near an optical fiber [158, 159], planar dielectric surface [160], nanosphere [161], and scanning near-field optical microscope tip [162]. In particular, the radiative properties of a molecule are shown to be significantly modified near metallic nanoparticles that support plasmon resonances [163, 164]. Furthermore, plasmon-mediated coupling through a thin metal film has been demonstrated [165].

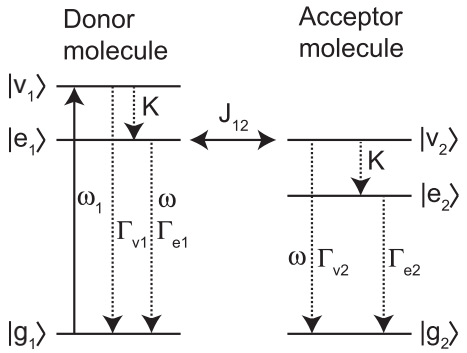

Figure 3: Energy-level diagram of the donor and acceptor molecules. The states $|e_1\rangle$ and $|v_2\rangle$ are coupled by the dipole-dipole interaction characterized by the coupling factor J_{12}. The parameters $\Gamma_{v1,v2}$ and $\Gamma_{e1,e2}$ denote the radiative decay rates from the excited states $|v_{1,2}\rangle$ and $|e_{1,2}\rangle$ to the ground states $|g_{1,2}\rangle$, whereas K denotes the non-radiative vibrational relaxation rate. Furthermore, the energy associated with the transitions $|e_1\rangle \rightarrow |g_1\rangle$ and $|v_2\rangle \rightarrow |g_2\rangle$ is $\hbar\omega$, and ω_1 is the angular frequency of the exciting light. [Paper V]

The fluorescence resonance energy transfer (FRET) between two molecules can be analyzed by considering the molecules as three-level systems [166] with energy-level diagrams depicted in Fig. 1. One of the molecules (the donor) is initially in an excited state and the other (the acceptor) in its ground state. The excitation energy is then transferred from the donor to the acceptor via a dipole-dipole coupling. The donor is excited to the state $|v_1\rangle$ by an incident optical field with angular frequency ω_1, while the acceptor is in its ground state $|g_2\rangle$. After internal relaxation, characterized by a (non-radiative) vibrational relaxation rate K, the donor resides in the excited state $|e_1\rangle$. The excited donor then couples by dipole-dipole interaction to the excited level $|v_2\rangle$ of the acceptor molecule. The dipole-dipole coupling factor J_{12} for two molecules has the form [166]

$$J_{12} = -\boldsymbol{\mu}_2 \cdot \overleftrightarrow{G}(\mathbf{r}_2, \mathbf{r}_1, \omega) \cdot \boldsymbol{\mu}_1, \tag{112}$$

where $\boldsymbol{\mu}_1$ and $\boldsymbol{\mu}_2$ are the dipole transition moments associated with the transitions between the levels $|e_1\rangle$ and $|g_1\rangle$, and $|v_2\rangle$ and $|g_2\rangle$, of the two molecules located at $\mathbf{r}_1$ and $\mathbf{r}_2$, respectively.

The dipole-dipole coupling strength associated with FRET in a system consisting of a chain of metallic nanoparticles can be enhanced at certain resonance frequencies [Paper V]. Moreover, in this particle-chain mediated coupling, the enhancement is strongly polarization sensitive. This is illustrated in Fig. 4 where the coupling strength $\Omega_{12} = \mathrm{Re}\{J_{12}\}/\hbar$ is shown for a straight particle chain consist-

ing of 11 silver particles (radius 10 nm) having a center-to-center distance of 30 nm. The donor and the acceptor molecules are placed at a distance of 20 nm from the opposite ends of the chain. The coupling is strongest when the dipole moments of the acceptor and donor molecules are parallel to the chain. [Paper V] The coupling re-

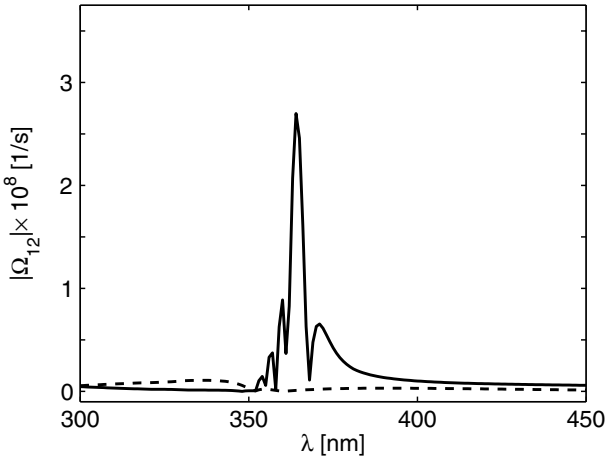

Figure 4: Coupling strengths as a function of the wavelength λ for donor and acceptor molecules which are oriented parallel (solid curve) and perpendicular (dashed curve) to the straight particle chain consisting of 11 silver particles of radius 10 nm. The center-to-center distance between the particles is 30 nm and the acceptor and donor molecules are located at a distance of 20 nm from the opposite ends of the chain. The coupling is strongest when the dipole moments of the acceptor and donor molecules are parallel to the chain. [Paper V]

mains fairly strong also for curved particle chains. The orientation sensitivity of the coupling can be utilized in a structure where the coupling to the different branches of the chain depends strongly on the orientation of the donor dipole. This can be of interest in developing optical components for plasmonics.

A more comprehensive picture of the interaction of electromagnetic field with molecules in complex environments can be achieved by combining the classical treatment of the field and the Green's function formalism with quantum-mechanical treatment of the molecules by employing optical Bloch equations [96].

5 Coherence properties of optical near fields

So far the optical coherence theory has been applied almost exclusively to far fields or planar waves such as (collimated) optical beams [24]. For these purposes the scalar or 2D electromagnetic theory is adequate. However, in analyzing optical near fields where the evanescent contribution is significant, the full 3D electromagnetic treatment is necessary. Recently, some of the concepts of traditional coherence theory, e.g., the degree of polarization and electromagnetic degree of coherence were extended to 3D electromagnetic fields (see Sec. 3). Furthermore, the first investigations on these quantities in optical near fields have appeared [22, Paper I, Paper IV].

The conventional wisdom in coherence theory is that the spatial correlations of an electromagnetic field extend, at least, over a distance on the order of the wavelength of light. This holds also for fields which are generated by highly incoherent sources such as thermal sources. However, in the conventional theory the role of evanescent waves, which are significant in the near field of the source, is ignored. In order to describe correctly the coherence properties of optical near fields, these waves must be taken into account. Indeed, recent theoretical studies indicate that the correlations in the optical near field of a thermal half-space source can be much shorter than the wavelength of light [19, 20]. The extraordinary short spatial coherence length originates from the evanescent waves and absorption of the source medium. In fact, recent theoretical work shows that there is no fundamental lower limit for the spatial coherence length inside a finite source region even if the medium is non-absorbing [167]. This result holds if the electromagnetic response of the material can be described as local. However, it has been demonstrated that there exists a physical minimum value for the coherence length of thermal electromagnetic fields near a planar surface [168]. This minimum coherence length is due to the non-local dielectric response of the material which becomes important on the scale of the electron mean free path [168].

In studies of coherence of optical near fields, thermal sources have obtained the most attention. The spatial coherence properties of thermal half-space sources show that the spatial correlations can be much shorter than the wavelength, or extend over a distance of several wavelengths [19, 20]. If the thermal source is composed of, e.g., slightly lossy glass, the field correlations in the immediate vicinity of the surface have the sinc-form which is characteristic for sources obeying Lambert's law, such as a black-body source [24]. For strongly absorbing medium, such as tungsten (W) at $\lambda = 500$ nm the correlation length very close to the surface is on the order of the skin depth of the metal. Farther away, where the contribution of the evanescent waves to the field becomes negligible, the field correlations assume the sinc form. The extremely short spatial correlation length close to the surface is explained by absorption over a skin-depth distance within the tungsten surface [19].

On the other hand, field correlations may extend over several tens of wavelengths, when resonant surface waves, such as surface plasmon or phonon polaritons, are excited [19, 20]. Thus, physically, the resonant surface waves mediate coherence. Studies of polarization properties in thermal near fields using the concept of 3D degree of polarization shows that surface polaritons can also create highly polarized thermal near fields [22]. In addition to the coherence and polarization properties, also the spectrum of the near field may differ from the source and far-field values, and the near field of a thermal source may even be quasimonochromatic when plasmon or phonon polaritons are excited. [21]. Based on these theoretical predictions, it has been experimentally demonstrated that by diffracting the surface-polariton field by a grating coupler etched on the source, highly coherent, directional emission from a thermal source can be obtained at certain wavelengths [169].

Spatial correlation lengths that are significantly shorter than the wavelength of light have been experimentally observed in optical near fields in the close proximity of highly scattering, randomly inhomogeneous media [170]. It has also been experimentally seen that the spatial coherence length in the near field depends on the distance from the surface. This dependence vanishes at several wavelengths away from the surface where the evanescent waves become negligible. These observations are consistent with the theoretical predictions discussed above.

The problems involved in measuring two-point correlations in near-field have also been theoretically addressed [171]. It has been shown that it is not possible to measure accurately spatial correlations of highly incoherent fields such as those which may exist in the near-field of thermal sources. The measurement of field correlations at two points requires the use of two near-field probes (dipoles). The probes scatter the evanescent field and the scattered field is then detected in the far zone. However, when the probes approach each other their interaction results in spurious correlations that are not present in the actual field. Thus there exists correlations in the measured signal that are artefact of the measurement apparatus. For typical parameter values, it is estimated that these correlations become important for distances $\leq 0.1\lambda$ [171].

The role of surface plasmons on planar surfaces has been shown to significantly affect the near field coherence properties. This suggests that also localized surface plasmons in metallic nanoparticles and nanowires can have a profound effect on the spatial coherence of the near field. Analysis of plasmon resonances in cylindrical nanowires shows a rich variety of electric-field correlation effects in the immediate near zone around the cylinders [Paper IV]. In particular, at the resonance wavelength the near field of the metal cylinder can become highly polarized and coherent, even if the illuminating field is highly incoherent. Figure 5 shows the spectral density, the 3D degree of polarization, and the electromagnetic degree of coherence for two interacting silver nanocylinders of radius 25 nm. The center-to-center distance between the cylinders is 55 nm and the wavelength of the illuminating 1D TM-

polarized Gaussian Schell-model beam is 375 nm. This corresponds to a resonance wavelength of the two cylinder configuration [136, 139]. It is also demonstrated that in chains of nanocylinders the degree of spatial coherence can influence the coupling of the incident field into the chain and alter the near- field intensity profile [Paper IV].

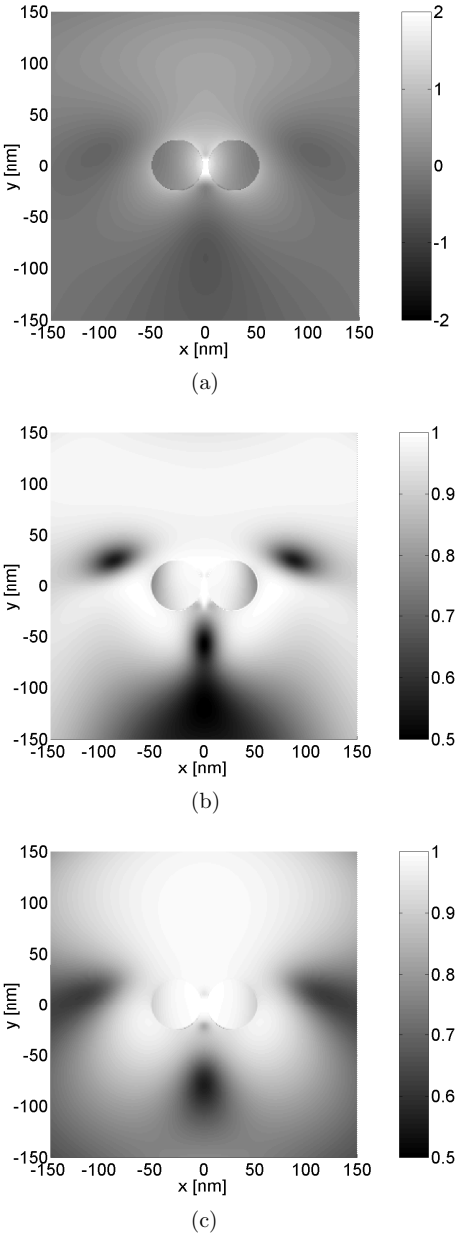

Figure 5: Illustration of the coherence properties of the near field around two interacting silver cylinders ($r = 25$ nm) with a center-to-center separation of 55 nm: (a) spectral density $\log_{10}[S(\mathbf{r}, \omega)]$ (arbitrary units), (b) 3D degree of polarization $P_3(\mathbf{r}, \omega)$, and (c) electromagnetic degree of coherence $\mu_{el}(\mathbf{r}, 0, \omega)$. The beam parameters of the incident (from above) 1D Gaussian Schell-model beam are $w_0 = 4.8\lambda$ and $\sigma_0 = 0.6\lambda$, and the wavelength of light is $\lambda = 375$ nm corresponding to the resonance of the structure. [Paper IV]

6 Summary and conclusions

The theory of coherence, in its classical and quantum-mechanical forms, constitutes the fundamental basis of optics. All sources and the fields that they generate fluctuate whether due to changes in the temperature, density and pressure of the medium, or due to reasons quantum mechanical in their origin. In order to be able to apply the theory in the domain of nanophotonics, it is necessary to take fully into account the polarization properties of light and to consider also non-planar fields. The presence of evanescent waves and surface excitations can make the coherence properties of optical near fields significantly differ from those in far-fields. This is a fact which needs to be paid attention to in nano-optics applications. The extension of the electromagnetic coherence theory to the realm of nano optics and photonics is thus of both fundamental and practical interest.

In this thesis, specific nano-optical systems have been studied with emphasis on the polarization and spatial coherence properties of the electromagnetic field. Both deterministic and statistical fields were considered. The recently introduced concepts of electromagnetic coherence theory for 3D fields were applied to study polarization and spatial coherence of fluctuating near fields. Also, an explicit form of the coherent-mode representation was for the first time derived for fully three-dimensional electromagnetic fields. The representation applies to fields whose electric cross-spectral density tensor is proportional to the imaginary part of the infinite-space Green tensor.

The thesis includes an investigation of the transmission of partially polarized light through a near-field probe. The concept of three-dimensional degree of polarization was applied to characterize the polarization of the electric field. The calculations which were based on the boundary-integral technique made use of a two-dimensional model for the probe tip. It was shown that there is a clear difference between the polarization properties of the transmitted and incident fields which result from the fact that TM-polarized light is better transmitted through the tip than TE-polarized light. For instance, a probe with a small opening angle and a small aperture acts like a polarizer blocking the TE component and thus resulting in a high degree of polarization for the transmitted field. Furthermore, a comparison of the 2D and 3D degrees of polarization in the far field shows that both parameters provide similar information about the polarization properties of the far field although they differ in their numerical values.

The boundary-integral technique was also applied to investigate the spectral properties of resonant transmission of light through a sub-wavelength slit in a thin metal film. The dependence of the transmitted spectrum on the geometry and material properties of the slit was analyzed. In particular, the resonance wavelength was shown to depend strongly on the material within the slit, and the shift of the resonance peak in the transmission spectrum is suggested to be useful for detection of

small changes in the refractive index of the medium in the slit. The boundary-integral technique was also combined with the coherent-mode representation to study plasmon resonances in cylindrical nanowires when the incident field is partially coherent. It was shown that the coherence properties of optical near fields can change at subwavelength scale. In particular, the near field of the metal cylinder can be highly polarized and coherent even if the illuminating field is highly incoherent. It was also demonstrated that in chains of nanocylinders the partial spatial coherence can influence the coupling of the incident field into the chain and alter the near field intensity profile, as well as the energy flow in the array.

The thesis also includes a study of the dipole-dipole coupling mediated by a chain of metal particles. The calculation which was based on the coupled-dipole method showed that the coupling strength can be enhanced at certain resonance frequencies and that it is strongly polarization sensitive: the coupling is strongest when the dipole moments of the acceptor and donor molecules are parallel to the chain. It is demonstrated that the orientation sensitivity of the coupling can be utilized in a structure where the orientation of the donor dipole decides to which of the different branches of the chain the coupling occurs.

In this thesis electromagnetic fields in specific nano-optical systems were considered. In particular, the partial polarization and partial coherence of optical near fields were studied in the context of two-dimensional systems, i.e., in a 2D-model of a SNOM probe and in a system of metallic nanowires. There exist so far relatively few studies on the spatial coherence properties of optical near fields. The extension of the previous investigations to fully three-dimensional geometries, i.e., to a 3D probe and to metallic nanoparticles, could provide further insight into the nature of partially coherent and partially polarized electromagnetic near fields. Furthermore, an analysis and detection of the coherence properties of optical near fields could lead to additional optical information which cannot be obtained by detecting only the intensity distribution with traditional SNOM techniques. For example, the detection of near-field Stokes parameters would result in supplementary information about the polarization statistics at the immediate vicinity of the source. Moreover, the fact that for certain sources the transverse spatial coherence length in the near field can be much shorter (and the longitudinal coherence length possibly longer) than the wavelength of light excites an idea of a new type of probing technique based on the coherence properties of electromagnetic fields. More precisely, probing the surface of such a source and detecting the interference between the light from the probe and the source, gives in principle, coherence-based information on the sample surface on the sub-wavelength scale as the transverse coherence length is much smaller than the wavelength. Furthermore, since the longitudinal coherence length exceeds the wavelength, the probe does not necessarily need to be at a sub-wavelength distance from the source. The recent publications and the work presented in this Thesis on electromagnetic coherence theory therefore suggest that the investigation of coherence properties could not only provide additional information on optical near fields, but possibly also provide basis for new applications in nanophotonics.

References

[1] L. Novotny and B. Hecht, *Principles of Nano-Optics* (Cambridge University Press, Cambridge, UK, 2006).

[2] P. N. Prasad, *Nanophotonics* (Wiley, New Jersey, 2004)

[3] M. Ohtsu and H. Hori, *Near-Field Nano-Optics: From Basic Principles to Nano-Fabrication and Nano-Photonics* (Kluwer, New York, 1999).

[4] D. Courjon, *Near-Field Micrsocopy and Near-Field Optics* (Imperial College Press, Singapore, 2003).

[5] J. P. Fillard, *Near-Field Optics and Nanoscopy* (World Scientific, Singapore, 1996).

[6] M. A. Paesler and P. J. Moyer, *Near-Field Optics: Theory, Instrumentation and Applications* (Wiley, New York, 1996).

[7] J.-J. Greffet and R. Carminati, "Image formation in near-field optics", Prog. Surf. Sci. **56**, 133–237 (1997).

[8] B. Hecht, B. Sick, U. P. Wild, V. Deckert, R. Zenobi, O. J. F. Martin, and D. W. Pohl, "Scanning near-field optical microscopy with aperture probes: Fundamentals and applications", J. Chem. Phys. **112**, 7761–7774 (2000).

[9] V. M. Agranovich and D. L. Mills, *Surface Polaritons* (North-Holland, Amsterdam, 1982).

[10] H. Raether, *Surface plasmons on smooth and rough surfaces and on gratings* (Springer, Berlin, 1988).

[11] W. L. Barnes, A. Dereux, and T. W. Ebbesen, "Surface plasmon subwavelength optics", Nature **424**, 824–830 (2003).

[12] A. V. Zayats, I. I. Smolyaninov, and A. A. Maradudin, "Nano-optics of surface plasmon polaritons", Phys. Rep. **408**, 131–314 (2005).

[13] E. Ozbay, "Plasmonics: merging photonics and electronics at nanoscale dimensions", Science **311**, 189–193 (2006).

[14] J. Homola, S. S. Yee, and G. Gauglitz, "Surface plasmon resonance sensors: review", Sensors Actuat. B **54**, 3–15 (1999).

[15] K. Kneipp, H. Kneipp, I. Itzkan, R. R. Dasari, and M. S. Field, "Surface enhanced Raman scattering and biophysics", J. Phys.: Condens. Matter **14**, R597–R624 (2002).

[16] R. R. Chance, A. Prock, and R. Silbey, "Molecular fluorescence and energy transfer near interfaces", in *Advances in Chemical Physics* Vol. 37, I. Prigogine and S. A. Rice, eds. (Wiley, 1978), pp. 1–65.

[17] G. W. Ford and W. H. Weber, "Electromagnetic interactions of molecules with metal surfaces", Phys. Rep. **113**, 195-287.

[18] W. L. Barnes, "Fluorescence near interfaces: the role of photonic mode density", J. Mod. Opt. **45**, 661–699 (1998).

[19] R. Carminati and J.-J. Greffet, "Near-field effects in spatial coherence of thermal sources", Phys. Rev. Lett. **82**, 1660–1663 (1999).

[20] C. Henkel, K. Joulain, R. Carminati, and J.-J. Greffet, "Spatial coherence of thermal near fields", Opt. Commun. **186**, 57–67 (2000).

[21] A. V. Shchegrov, K. Joulain, R. Carminati, and J.-J. Greffet, "Near-field spectral effects due to electromagnetic surface excitations", Phys. Rev. Lett. **85**, 1548–1551 (2000).

[22] T. Setälä, M. Kaivola, and A. T. Friberg, "Degree of polarization in near fields of thermal sources: effects of surface waves", Phys. Rev. Lett. **88**, 123902 (2002).

[23] M. Born and E. Wolf, *Principles of Optics*, 7th Ed. (Cambridge University Press, Cambridge, UK, 1999).

[24] L. Mandel and E. Wolf, *Optical Coherence and Quantum Optics* (Cambridge University Press, Cambridge, UK, 1995).

[25] J. Peřina, *Coherence of Light* (Reidel, Dordrecht, 1985).

[26] J. W. Goodman, *Statistical Optics* (Wiley, New York, 1985).

[27] C. Brosseau, *Fundamentals of Polarized Light: A Statistical Optics Approach* (Wiley, New York, 1998).

[28] J. D. Jackson, *Classical Electrodynamics*, 3rd Ed., (Wiley, New York, 1999).

[29] P. J. Feibelman, "Surface electromagnetic fields", Prog. Surf. Sci. **12**, 287–408 (1982).

[30] G. W. Hanson and A. B. Yakovlev, *Operator Theory for Electromagnetics: An Introduction* (Springer, New York, 2002).

[31] C.-T. Tai, *Dyadic Green's Functions in Electromagnetic Theory* (Intext, Scranton, PA, 1971).

[32] A. D. Yaghjian, "Electric dyadic Green's functions in the source region", Proc. IEEE **68**, 248–263 (1980).

[33] J. Van Bladel, "Some remarks on Green's dyadic for infinite space", IRE Trans. Antennas Propagat. **9**, 563–566 (1961).

[34] L. Novotny, B. Hecht, and D. W. Pohl, "Interference of locally excited surface plasmons", J. Appl. Phys. **81**, 1798–1806 (1997).

[35] M. Ohtsu and K. Kobayashi, *Optical Near Fields: Introduction to Classical and Quantum Theories of Electromagnetic Phenomena at the Nanoscale* (Springer, Berlin, 2004).

[36] W. C. Chew, "Introduction to Electromagnetic Analysis and Computational Electromagnetics", in *Fast and Efficient Algorithms in Computational Electromagnetics*, W. C. Chew, J.-J. Jin, E. Michielssen, and J. Song, eds. (Artech House, Boston, 2001), pp. 1–76.

[37] J. Van Bladel, *Electromagnetic Fields* (Hemisphere, Washington, 1985).

[38] J. Wiersig, "Boundary element method for resonances in dielectric microcavities", J. Opt. A **5**, 53–60 (2003).

[39] C. F. Bohren and D. R. Huffman, *Absorption and Scattering of Light by Small Particles* (Wiley, New York, 1983).

[40] M. Abramowitz and I. A. Stegun, eds., *Handbook of Mathematical Functions* (Dover, New York, 1972).

[41] C. A. Brebbia, J. F. C. Telles, and L. C. Wrobel, *Boundary element techniques: theory and applications in engineering* (Springer, Berlin, 1984).

[42] P. K. Banerjee and R. Butterfield, *Boundary element methods in engineering science* (McGraw-Hill, London, 1981).

[43] L. Ram-Mohan and L. Ramdas, *Finite Element and Boundary Element Applications in Quantum Mechanics* (Oxford University Press, Oxford, 2002).

[44] R. F. Harrington, *Field computation by moment methods* (The Macmillan Company, New York, 1968).

[45] S. Kagami and I. Fukai, "Application of boundary-element method to electromagnetic field problems", IEEE Trans. Microwave Theory Tech. **32**, 455–461 (1984).

[46] M. Koshiba and M. Suzuki, "Application of boundary-element method to waveguide discontinuities", IEEE Trans. Microwave Theory Tech. **34**, 301–307 (1986).

[47] A. Madrazo and M. Nieto-Vesperinas, "Surface structure and polariton interactions in the scattering of electromagnetic waves from a cylinder in front of a conducting grating: theory for the reflection photon scanning tunneling microscope", J. Opt. Soc. Am. A **13**, 785–795 (1996).

[48] K. Tanaka, M. Tanaka, and T. Omoya, "Boundary integral equations for a two-dimensional simulator of a photon scanning tunneling microscope", J. Opt. Soc. Am. A **15**, 1918–1931 (1998).

[49] C. M. Kelso, P. D. Flammer, J. A. DeSanto, and R. T. Collins, "Integral equations applied to wave propagation in two dimensions: modeling the tip of a near-field scanning optical microscope", J. Opt. Soc. Am. A **18**, 1993–2001 (2001).

[50] M. Nieto-Vesperinas, *Scattering and Diffraction in Physical Optics* (Wiley, New York, 1991).

[51] P. A. Knipp and T. L. Reinecke, "Boundary-element method for the calculation of electronic states in semiconductor nanostructures", Phys. Rev. B **54**, 1880–1891 (1996).

[52] I. Kosztin and K. Schulten, "Boundary integral method for stationary states of two-dimensional quantum systems", Int. J. Mod. Phys. C **8**, 293–325 (1997).

[53] J. C. F. Telles, "A self-adaptive co-ordinate transformation for efficient numerical evaluation of general boundary integrals", Int. J. Numer. Meth. Eng. **24**, 959–973 (1987).

[54] J. Jin, *The Finite Element Method in Electromagnetics*, 2nd Ed. (Wiley, New York, 2002).

[55] A. Taflove and S. C. Hagness, *Computational Electrodynamics: The Finite-Difference Time-Domain Method*, 3rd Ed. (Artech House, Boston, MA, 2005).

[56] A. J. Poggio and E. K. Miller, "Integral equation solutions of three dimensional scattering problems", in *Computer Techniques for Electromagnetics*, R. Mitra, ed. (Pergamon, New York, 1973), pp. 159–264.

[57] J. A. Stratton, *Electromagnetic Theory* (McGraw Hill, New York, 1941).

[58] V. Twersky, "Multiple scattering of electromagnetic waves by arbitrary configurations", J. Math. Phys. **8**, 589–610 (1967).

[59] M. Guiggiani and A. Gigante, "A general algorithm for multidimensional Cauchy principal value integrals in the boundary element method", ASME J. Appl. Mech. **57**, 906–915 (1990).

[60] M. Guiggiani, "Computing principal-value integrals in 3D BEM for time-harmonic elastodynamics - a direct approach", Commun. Appl. Numer. Meth. **8**, 141–149 (1992).

[61] S. V. Tsinopoulos, S. E. Kattis, and D. Polyzos, "Three-dimensional boundary element analysis of electromagnetic wave scattering by penetrable bodies", Computational Mech. **21**, 306–315 (1998).

[62] E. Wolf, "New theory of partial coherence in the space-frequency domain. Part I: spectra and cross spectra of steady-state sources", J. Opt. Soc. Am. **72**, 343–351 (1982).

[63] J. Tervo, T. Setälä, and A. T. Friberg, "Theory of partially coherent electromagnetic fields in the space-frequency domain", J. Opt. Soc. Am. A **21**, 2205–2215 (2004).

[64] T. Setälä, A. Shevchenko, M. Kaivola, and A. T. Friberg, "Degree of polarization for optical near fields", Phys. Rev. E **66**, 016615 (2002).

[65] T. Setälä, *Spatial correlations and partial polarization in electromagnetic fields: effects of evanescent waves*, D.Sc. dissertation (Helsinki University of Technology, Espoo, 2003).

[66] J. C. Samson, "Descriptions of the polarization states of vector processes: applications to ULF magnetic fields", Geophys. J. R. Astr. Soc. **34**, 403–419 (1973).

[67] R. Barakat, "Degree of polarization and the principal idempotents of the coherency matrix", Opt. Commun. **23**, 147–150 (1977).

[68] A. Luis, "Degree of polarization for three-dimensional fields as a distance between correlation matrices", Opt. Commun. **253**, 10–14 (2005).

[69] T. Setälä, K. Lindfors, M. Kaivola, J. Tervo, and A. T. Friberg, "Intensity fluctuations and degree of polarization in three-dimensional thermal light fields", Opt. Lett. **29**, 2587–2589 (2004).

[70] C. Brosseau and A. Dogariu, "Symmetry and polarization descriptors for an arbitrary electromagnetic wavefield" in *Progress in Optics* Vol. 49, E. Wolf ed. (Elsevier, 2006), pp. 315–380.

[71] A. Luis, "Quantum polarization for three-dimensional fields via Stokes operators", Phys. Rev. A **71**, 023810 (2005).

[72] A. Luis, "Degree of polarization in quantum optics", Phys. Rev. A **66**, 013806 (2002).

[73] J. Lehner, U. Leonhardt, and H. Paul, "Unpolarized light: classical and quantum states", Phys. Rev. A **53**, 2727–2735 (1996).

[74] K. Lindfors, T. Setälä, M. Kaivola, and A. T. Friberg, "Degree of polarization in tightly focused optical fields", J. Opt. Soc. Am. A **22**, 561–568 (2005).

[75] K. Lindfors, A. Priimagi, T. Setälä, A. Shevchenko, A. T. Friberg, and M. Kaivola, "Local polarization of tightly focused unpolarized light", Nature Photonics **1**, 228–230 (2007).

[76] B. Karczewski, "Coherence theory of the electromagnetic field", Nuovo Cimento **30**, 906–915 (1963).

[77] E. Wolf, "Unified theory of coherence and polarization of random electromagnetic fields", Phys. Lett. A **312**, 263–267 (2003).

[78] J. Tervo, T. Setälä, and A. T. Friberg, "Degree of coherence for electromagnetic fields", Opt. Express **11**, 1137–1143 (2003).

[79] T. Setälä, J. Tervo, and A. T. Friberg, "Complete electromagnetic coherence in the space-frequency domain", Opt. Lett. **29**, 328–330 (2004).

[80] A. T. Friberg, "Electromagnetic Theory of Optical Coherence", in *Tribute to Emil Wolf: Science and Engineering Legacy of Physical Optics*, T. P. Jannson, ed. (SPIE, Bellingham, 2005), pp. 95–112.

[81] E. Wolf, "Comment on 'Complete electromagnetic coherence in the space-frequency domain' ", Opt. Lett. **29**, 1712 (2004).

[82] T. Setälä, J. Tervo, and A. T. Friberg, "Reply to comment on 'Complete electromagnetic coherence in the space-frequency domain' ", Opt. Lett. **29**, 1713–1714 (2004).

[83] E. Wolf, "Comment on a paper 'Radiation from arbitrarily polarized spatially incoherent source' ", Opt. Commun. **242**, 321–322 (2004).

[84] T. Saastamoinen, J. Tervo, and J. Turunen, "Reply to comment on 'Radiation from arbitrarily polarized spatially incoherent planar sources' ", Opt. Commun. **242**, 323–325 (2004).

[85] T. Setälä, J. Tervo, and A. T. Friberg, "Stokes parameters and polarization contrasts in Young's interference experiment", Opt. Lett. **31**, 2208–2210 (2006).

[86] T. Setälä, J. Tervo, and A. T. Friberg, "Contrasts of Stokes parameters in Young's interference experiment and electromagnetic degree of coherence", Opt. Lett. **31**, 2669-2671 (2006).

[87] R. J. Glauber, "The quantum theory of optical coherence", Phys. Rev. **130**, 2529–2539 (1963).

[88] F. Gori, M. Santarsiero, R. Simon, G. Piquero, R. Borghi, and G. Guattari, "Coherent-mode decomposition of partially polarized, partially coherent sources", J. Opt. Soc. Am. A **20**, 78–84 (2003).

[89] D. Cabaret, S. Rossano, and C. Brouder, "Mie scattering of a partially coherent beam", Opt. Commun. **150**, 239–250 (1998).

[90] S. Withington, G. Yassin, J. A. Murphy, "Dyadic analysis of partially coherent submillimeter-wave antenna systems", IEEE Trans. Antennas Propag. **49**, 1226–1234 (2001).

[91] J. Huttunen, A. T. Friberg, and J. Turunen, "Scattering of partially coherent electromagnetic fields by microstructured media", Phys. Rev. E **52**, 3081–3092 (1995).

[92] J. M. Vigoureux and D. Courjon, "Detection of nonradiative fields in light of the Heisenberg uncertainty principle and the Rayleigh criterion", Appl. Opt. **31**, 3170–3177 (1992).

[93] F. de Fornel, P. M. Adam, L. Salomon, J. P. Goudonnet, A. Sentenac, R. Carminati, and J.-J. Greffet, "Analysis of image formation with a photon scanning tunneling microscope", J. Opt. Soc. Am. A **13**, 35–45 (1996).

[94] R. Carminati and J.-J. Greffet "Influence of dielectric contrast and topography on the near field scattered by an inhomogeneous surface", J. Opt. Soc. Am. A **12**, 2716–2725 (1995).

[95] C. Girard and A. Dereux, "Near-field optics theories", Rep. Prog. Phys. **59**, 657–699 (1996).

[96] C. Girard, "Near fields in nanostructures", Rep. Prog. Phys. **68**, 1883–1933 (2005).

[97] G. W. Bryant, "Probing quantum nanostructures with near-field optical microscopy and vice versa", Appl. Phys. Lett. **72**, 768–770 (1998).

[98] P. Blattner, H. P. Herzig, and R. Dändliker, "Scanning near-field optical microscopy: transfer function and resolution limit", Opt. Commun. **155**, 245–250 (1998).

[99] L. Novotny, D. W. Pohl, and P. Regali, "Light propagation through nanometer-sized structures: the two-dimensional-aperture scanning near-field optical microscope", J. Opt. Soc. Am. A **11**, 1768–1779 (1994).

[100] L. Novotny, D. W. Pohl, and B. Hecht, "Light confinement in scanning near-field optical microscopy", Ultramicroscopy **61**, 1–9 (1995).

[101] H. Furukawa and S. Kawata, "Analysis of image formation in a near-field scanning optical microscope: effects of multiple scattering", Opt. Commun. **132**, 170–178 (1996).

[102] E. Vasilyeva and A. Taflove, "Three-dimensional modeling of amplitude-object imaging in scanning near-field optical microscopy", Opt. Lett. **23**, 1155–1157 (1998).

[103] O. J. F. Martin, C. Girard, and A. Dereux, "Generalized field propagator for electromagnetic scattering and light confinement", Phys. Rev. Lett. **74**, 526–529 (1995).

[104] O. J. F. Martin, C. Girard, and A. Dereux, "Dielectric versus topographic contrast in near-field microscopy", J. Opt. Soc. Am. A **13**, 1801–1808 (1996).

[105] O. J. F. Martin, "3D simulations of the experimental signal measured in near-field optical microscopy", J. Microsc. **194**, 235–239 (1999).

[106] R. D. Grober, R. J. Schoellkopf, and D. E. Prober, "Optical antenna: towards a unity efficiency near-field optical probe" Appl. Phys. Lett. **70**, 1354–1356 (1997).

[107] A. Nesci, R. Dändliker, M. Salt, and H. P. Herzig, "Measuring amplitude and phase distribution of fields generated by gratings with sub-wavelength resolution", Opt. Commun. **205**, 229–238 (2002).

[108] L. Vaccaro, L. Aeschimann, U. Staufer, H. P. Herzig, and R. Dändliker, "Propagation of the electromagnetic field in fully coated near-field optical probes", Appl. Phys. Lett. **83**, 584–586 (2003).

[109] R. Dändliker, P. Tortora, L. Vaccaro, and A. Nesci, "Measuring three-dimensional polarization with scanning optical probes", J. Opt. A: Pure Appl. Opt. **6**, S18-S23 (2004).

[110] P. Tortora, R. Dändliker, W. Nakagawa, and L. Vaccaro, "Detection of non-paraxial optical fields by optical fiber tip probes", Opt. Commun. **259**, 876–882 (2006).

[111] T. W. Ebbesen, H. J. Lezec, H. F. Ghaemi, T. Thio, and P. A. Wolff, "Extraordinary optical transmission through sub-wavelength hole arrays", Nature **391**, 667–669 (1998).

[112] U. Schröter and D. Heitmann, "Surface-plasmon-enhanced transmission through metallic gratings", Phys. Rev. B **58**, 15419–15421 (1998).

[113] J. A. Porto, F. J. García-Vidal, and J. B. Pendry, "Transmission resonances on metallic gratings with very narrow slits", Phys. Rev. Lett. **83**, 2845–2848 (1999).

[114] E. Popov, M. Nevière, S. Enoch, and R. Reinisch, "Theory of light transmission through subwavelength periodic hole arrays", Phys. Rev. B **62**, 16100–16108 (2000).

[115] L. Salomon, F. Grillot, A. Zayats, and F. de Fornel, "Near-field distribution of optical transmission of periodic subwavelength holes in a metal film," Phys. Rev. Lett. **86**, 1110–1113 (2001).

[116] L. Martín-Moreno, F . J. García-Vidal, H. J. Lezec, K. M. Pellerin, T. Thio, J. B. Pendry, and T. W. Ebbesen, "Theory of extraordinary optical transmission through subwavelength hole arrays", Phys. Rev. Lett. **86**, 1114–1117 (2001).

[117] B. Dragnea, J. M. Szarko, S. Kowarik, T. Weimann, J. Feldmann, and S. R. Leone, "Near-field surface plasmon excitation on structured gold films", Nano Lett. **3**, 3–7 (2003).

[118] Ph. Lalanne, J. P. Hugonin, S. Astilean, M. Palamaru, and K. D. Möller, "One-mode model and Airy-like formulae for one-dimensional metallic gratings", J. Opt. A: Pure Appl. Opt. **2**, 48–51 (2000).

[119] S. Astilean, Ph. Lalanne, and M. Palamaru, "Light transmission through metallic channels much smaller than the wavelength", Opt. Commun. **175**, 265–273 (2000).

[120] S. Collin, F. Pardo, R. Teissier, and J.-L. Pelouard, "Strong discontinuities in the complex photonic band structure of transmission metallic gratings" Phys. Rev. B **63**, 033107 (2001).

[121] Q. Cao and Ph. Lalanne, "Negative role of surface plasmons in the transmission of metallic gratings with very narrow Slits", Phys. Rev. Lett. **88**, 057403 (2002).

[122] M. M. Treacy, "Dynamical diffraction in metallic optical gratings", Appl. Phys. Lett. **75**, 606–608 (1999).

[123] M. M. Treacy, "Dynamical diffraction explanation of the anomalous transmission of light through metallic gratings", Phys. Rev. B **66**, 195105 (2002).

[124] N. Bonod, S. Enoch, L. Li, E. Popov, and M. Nevière, "Resonant optical transmission through thin metallic films with and without holes", Opt. Express **11**, 482–490 (2003).

[125] Y. Takakura, "Optical resonance in a narrow slit in a thick metallic screen", Phys. Rev. Lett. **86**, 5601–5603 (2001).

[126] T. Thio, K. M. Pellerin, R. A. Linke, H. J. Lezec, and T. W. Ebbesen, "Enhanced light transmission through a single subwavelength aperture", Opt. Lett. **26**, 1972–1974 (2001).

[127] F. Yang and J. R. Sambles, "Resonant transmission of microwaves through a narrow metallic slit", Phys. Rev. Lett. **89**, 063901 (2002).

[128] A. P. Hibbins, J. R. Sambles, and C. R. Lawrence, "Gratingless enhanced microwave transmission through a subwavelength aperture in a thick metal plate", Appl. Phys. Lett. **81**, 4661–4663 (2002).

[129] F. J. García-Vidal, H. J. Lezec, T. W. Ebbesen and L. Martín-Moreno, "Multiple paths to enhance optical transmission through a single subwavelength slit", Phys. Rev. Lett. **90**, 213901 (2003).

[130] F. I. Baida, D. Van Labeke, and B. Guizal, "Enhanced confined light transmission by single subwavelength apertures in metallic films", Appl. Opt. **42**, 6811–6815 (2003).

[131] T. Vallius, J. Turunen, M. Mansuripur, and S. Honkanen, "Transmission through single subwavelength apertures in thin metal films and effects of surface plasmons", J. Opt. Soc. Am. A **21**, 456–463 (2004).

[132] I. P. Kaminow, W. L. Mammel, and H. P. Weber, "Metal-clad optical waveguides: analytical and experimental study", Appl. Opt. **13**, 396–405 (1974).

[133] H. J. Lezec, A. Degiron, E. Devaux, R. A. Linke, L. Martin-Moreno, F. J. Garcia-Vidal, and T. W. Ebbesen, "Beaming light from a subwavelength aperture", Science **297**, 820–822 (2002).

[134] L. Martín-Moreno, F. J. Garcia-Vidal, H. J. Lezec, A. Degiron, and T. W. Ebbesen, "Theory of highly directional emission from a single subwavelength aperture surrounded by surface corrugations", Phys. Rev. Lett. **90**, 167401 (2003).

[135] J. P. Kottmann, O. J. F. Martin, D. R. Smith, and S. Shultz, "Plasmon resonances of silver nanowires with a nonregular cross section", Phys. Rev. B **64**, 235402 (2001).

[136] J. P. Kottmann and O. J. F. Martin, "Plasmon resonant coupling in metallic nanowires", Opt. Express **8**, 655–663 (2001).

[137] S. K. Gray and T. Kupka, "Propagation of light in metallic nanowire arrays: finite-difference time-domain studies of silver cylinders", Phys. Rev. B **68**, 045415 (2003).

[138] C. Rockstuhl, M. G. Salt, and H. P. Herzig, "Application of the boundary-element method to the interaction of light with single and coupled metallic nanoparticles", J. Opt. Soc. Am. A **20**, 1969–1973 (2003).

[139] C. Rockstuhl, M. G. Salt and H. P. Herzig, "Analyzing the scattering properties of coupled metallic nanoparticles", J. Opt. Soc. Am. A **21**, 1761–1768 (2004).

[140] J.-W. Liaw, "Simulation of surface plasmon resonance of metallic nanoparticles by the boundary-element method", J. Opt. Soc. Am. A **23**, 108-116 (2006).

[141] M. Quinten, A. Leitner, J. R. Krenn, and F. R. Aussenegg, "Electromagnetic energy transport via linear chains of silver nanoparticles", Opt. Lett. **23**, 1331–1333 (1998).

[142] J. R. Krenn, A. Dereux, J. C. Weeber, E. Bourillot, Y. Lacroute, J. P. Goudonnet, G. Schider, W. Gotschy, A. Leitner, F. R. Aussenegg, and C. Girard, "Squeezing the optical near-field zone by plasmon coupling of metallic nanoparticles", Phys. Rev. Lett. **82**, 2590–2593 (1999).

[143] M. L. Brongersma, J. W. Hartman, and H. A. Atwater, "Electromagnetic energy transfer and switching in nanoparticle chain arrays below the diffraction limit", Phys. Rev. B **62**, R16356-R16359 (2000).

[144] S. A. Maier, M. L. Brongersma, P. G. Kik, and H. A. Atwater, "Observation of near-field coupling in metal nanoparticle chains using far-field polarization spectroscopy", Phys. Rev. B **65**, 193408 (2002).

[145] C. Girard and R. Quidant, "Near-field optical transmittance of metal particle chain waveguides", Opt. Express **12**, 6141–6146 (2004).

[146] J.-C. Weeber, A. Dereux, C. Girard, J. R. Krenn, and J.-P. Goudonnet, "Plasmon polaritons of metallic nanowires for controlling submicron propagation of light", Phys. Rev. B **60**, 9061–9068 (1999).

[147] G. Schider, J. R. Krenn, W. Gotschy, B. Lamprecht, H. Ditlbacher, A. Leitner, and F. R. Aussenegg, "Optical properties of Ag and Au nanowire gratings", J. Appl. Phys. **90**, 3825–3830 (2001).

[148] G. Schider, J. R. Krenn, A. Hohenau, H. Ditlbacher, A. Leitner, F. R. Aussenegg, W. L. Schaich, I. Puscasu, B. Monacelli, and G. Boreman, "Plasmon dispersion relation of Au and Ag nanowires", Phys. Rev. B **68**, 155427 (2003).

[149] G. Colas des Francs, C. Girard, J.-C. Weeber, and A. Dereux, "Near field optical adressing of single molecules in coplanar geometry: a theoretical study", J. Microsc. **202**, 307–312 (2001).

[150] W. Nomura, T. Yatsui, and M. Ohtsu, "Efficient optical near-field energy transfer along an Au nanodot coupler with size-dependent resonance", Appl. Phys. B **84**, 257–259 (2006).

[151] E. M. Purcell, "Spontaneous emission probabilities at radio frequencies", Phys. Rev. **69**, 681 (1946).

[152] G. S. Agarwal and S. D. Gupta, "Microcavity-induced modification of the dipole-dipole interaction", Phys. Rev. A **57**, 667–670 (1998).

[153] P. Andrew and W. L. Barnes, "Förster energy transfer in an optical microcavity", Science **290**, 785–788 (2000).

[154] D. M. Basko, F. Bassani, G.C. La Rocca, and V. M. Agranovich, "Electronic energy transfer in a microcavity", Phys. Rev. B. **62**, 15962 (2000).

[155] C. R. Bennett, J. B. Kirk, and M. Babiker, "Green-function theory of spontaneous emission and cooperative effects in a superlattice of thin metal layers", Phys. Rev. A **63**, 63812 (2001).

[156] R. L. Hartman and P. T. Leung, "Dynamical theory for modeling dipole-dipole interactions in a microcavity: the Green dyadic approach", Phys. Rev. B **64**, 193308 (2001).

[157] C. E. Finlayson, D. S. Ginger, and N. C. Greenham, "Enhanced Förster energy transfer in organic/inorganic bilayer optical microcavities", Chem. Phys. Lett. **338**, 83–87 (2001).

[158] X. M. Hua and J. I. Gersten, "Enhanced energy transfer between donor and acceptor molecules near a long wire or fiber", J. Chem. Phys. **91**, 1279–1286 (1989).

[159] F. Le Kien, S. D. Gupta, K. P. Nayak, and K. Hakuta, "Nanofiber-mediated radiative transfer betweeen two distant atoms", Phys. Rev. A **72**, 063815 (2006).

[160] M. Cho and R. J. Silbey, "Suppression and enhancement of van der Waals interactions", J. Chem. Phys. **104**, 8730–8741 (1996).

[161] V. V. Klimov and V. S. Letokhov, "Resonance interaction between two atomic dipoles separated by the surface of a dielectric nanosphere", Phys. Rev. A **58**, 3235–3247 (1998).

[162] C. Girard, O. J. F. Martin, G. Lévèque, G. Colas des Francs, and A. Dereux, "Generalized bloch equations for optical interactions in confined geometries", Chem. Phys. Lett. **404**, 44–48 (2005).

[163] P. Anger, P. Bharadwaj, and L. Novotny, "Enhancement and quenching of single-molecule fluorescence", Phys. Rev. Lett. **96**, 113002 (2006).

[164] R. Carminati, J.-J. Greffet, C. Henkel, and J. M. Vigoureux, "Radiative and non-radiative decay of a single molecule close to a metallic nanoparticle", Opt. Commun. **261**, 368–375 (2006).

[165] P. Andrew and W. L. Barnes, "Energy transfer across a metal film mediated by surface plasmon polaritons", Science **306**, 1002–1005 (2004).

[166] G. Colas des Francs, C. Girard, and O. J. F. Martin, "Fluorescence resonant energy transfer in the optical near field", Phys. Rev. A **67**, 053805 (2003).

[167] K. Blomstedt, T. Setälä, and A. T. Friberg, "Arbitrarily short coherence length in wave fields within finite lossless source regions", Phys. Rev. E **75**, 026610 (2007).

[168] C. Henkel and K. Joulain, "Electromagnetic field correlations near a surface with a nonlocal optical response", Appl. Phys. B **84**, 61–68 (2006).

[169] J.-J. Greffet, R. Carminati, K. Joulain, J.-P. Mulet, S. Mainguy, and Y. Chen, "Coherent emission of light by thermal sources", Nature **416**, 61–64 (2002).

[170] A. Apostol and A. Dogariu, "Spatial correlations in the near field of random media", Phys. Rev. Lett. **91**, 093901 (2003).

[171] J. Grondalski and D. F. V. James, "Is there a fundamental limitation on the measurement of spatial coherence for highly incoherent fields?", Opt. Lett. **28**, 1630–1632 (2003).

Abstracts of Publications I-V

I. We analyze the changes in the partial polarization of random, stationary light fields in transmission through a near-field probe. The probe is modelled as a two-dimensional metal-coated optical fiber tip through which the field is propagated by applying the boundary-integral method. Both the magnitude of the opening angle and the aperture size of the probe are found to significantly influence the partial polarization of the field. We discuss the results in terms of both the conventional two-dimensional and the recent three-dimensional formalism for the degree of polarization.

II. We analyze the spectral properties of resonant transmission of light through a sub-wavelength slit in a metal film. We show that the enhanced transmission can be understood in terms of interfering surface-wave-like modes propagating in the slit. We characterize the effect of geometrical and material properties of the slit on the transmission spectrum. Furthermore, we show that the wavelength of the transmission resonance strongly depends on the surrounding medium. This effect may be utilized in sensors, imaging, and the detection of, e.g. biomolecules.

III. It is known that statistically stationary, homogeneous, and isotropic source distributions generate, in an unbounded low-loss medium, an electromagnetic field whose electric cross-spectral density tensor is proportional to the imaginary part of the infinite-space Green tensor. Using the recently established electromagnetic theory of coherent modes we construct, in a finite spherical volume, the coherent-mode representation of the random electromagnetic field having this property. The analysis covers the fundamental case of blackbody radiation but is valid more generally; since a thermal equilibrium condition is not invoked, the electromagnetic field may have any spectral distribution. Within the scalar theory of coherent modes, which has been available for more than two decades, the analogous formulation results in the first explicit three-dimensional coherent-mode representation.

IV. We study the scattering of a partially coherent electromagnetic beam from metallic nanocylinders and analyze the effects of plasmon resonances on the coherence and polarization properties of the optical near field. We employ the coherent-mode representation for the incident field and solve the scattering problem independently for each mode using a boundary-integral method. Our results show that the plasmon resonances may significantly affect the coherence and polarization characteristics of the near field, and that partial coherence influences the energy flow in nanocylinder arrays.

V. We study the dipole-dipole coupling between two fluorescent molecules in the presence of a chain of metallic nanoparticles. We analyze the spectral behavior of the coupling strength and its dependence on the molecular orientation. Our results show that for certain resonant wavelengths the coupling strength between the molecules is greatly enhanced and is strongly polarization sensitive. We also demonstrate how metallic nanoparticles can be utilized in implementing a polarization-sensitive coupler.

ISBN 978-951-22-9026-0
ISBN 978-951-22-9027-7 (PDF)
ISSN 1795-2239
ISSN 1795-4584 (PDF)